Probabilistic fatigue analysis on a central holed thick steel plate of C1 Wedge Connection for wind turbine tower assembling

Liao, Ding; Cheng, Lu; Correia, José; Veljkovic, Milan; Zhu, Shun Peng; Winkes, Jasper; Creusen, Koen; Berto, Filippo

DOI
10.1016/j.oceaneng.2023.116328

Publication date
2023

Document Version
Final published version

Published in
Ocean Engineering

Ocean Engineering 290 (2023) 116328

Contents lists available at ScienceDirect

Ocean Engineering

journal homepage: www.elsevier.com/locate/oceaneng

Probabilistic fatigue analysis on a central holed thick steel plate of C1 Wedge Connection for wind turbine tower assembling

Ding Liao [a,b,c], Lu Cheng [a], José Correia [a,b,*], Milan Veljkovic [a], Shun-Peng Zhu [c], Jasper Winkes [d], Koen Creusen [d], Filippo Berto [e]

[a] Faculty of Civil Engineering and Geosciences, Delft University of Technology, Delft, 2628 CN, the Netherlands
[b] INEGI & CONSTRUCT, Faculty of Engineering, University of Porto, Porto, 4200-465, Portugal
[c] School of Mechanical and Electrical Engineering, University of Electronic Science and Technology of China, Chengdu, 611731, China
[d] C1 Connections, Hague, 2596 AL, the Netherlands
[e] Department of Chemical Engineering, La Sapienza University of Rome, Rome, Italy

ARTICLE INFO

Handling Editor: Prof. A.I. Incecik

Keywords:
Thick steel plate
Central hole
Manufacturing defect
Surface size effect
Probabilistic fatigue
Life prediction

ABSTRACT

Hole patterns are common in engineering design for connections and/or assembly purposes. Geometrical discontinuities can cause stress concentration in localized areas, making them more prone to fatigue crack initiation and influencing the fatigue life of the overall unit. In the past, much effort has been exerted on fatigue modelling of holed plates from both experimental and theoretical perspectives. However, most studied objects were aluminium or titanium thin plates for aviation purposes. In this work, the fatigue performance of a downscaled holed thick steel plate, extracted from a novel C1 Wedge Connection for wind turbine tower assembling, was tested and categorized according to commonly used industry codes. In particular, the influence of the surface size effect was experimentally observed and computationally discussed. Finally, a probabilistic fatigue model was proposed, which gives a favourable prediction on the fatigue behaviour of the surface polished holed thick steel plate with the help of the Smith–Watson–Topper (SWT) model.

1. Introduction

In industries such as mechanical, civil, chemical, energy, and aviation, large-scale structural systems are often fabricated in multiple segments, which are later assembled at installation sites. In this way, the costs and difficulties in manufacturing and transportation can be significantly reduced. For assembling metal segments, welding, riveting and bolting are three principal manners. In particular, for the cases without strict requirements on watertightness and/or airtightness, riveting and bolting are better options for their advantages in site operation, regular maintenance, and potential replacement, despite their comparatively higher costs (Alencar et al., 2019).

For components subjected to cyclic loadings, a core concern to their structural integrity is fatigue performance (Rozumek, 2009). A practical consideration for choosing rivet or bolt joints is their higher fatigue resistance than welded joints, as shown by experimental evidence (Valtinat and Hadrych, 2000; Chakherlou et al., 2010). However, both riveting and bolting require the prefabrication or drilling of holes in the segments. Together with groove, keyseat, etc., these geometrical discontinuities are collectively named "notch" in fatigue modelling (Liao et al., 2020a). Notch patterns are significant challenges to structural strength design due to their stress/strain concentrating effects under external cyclic loading, which accelerate crack initiation, propagation and final failure. Holed parts are particularly susceptible to fatigue crack initiation and premature failure due to the rough surface and manufacturing defects typically present at hole edges, which can be challenging to control during processing and quality control (Chakherlou and Vogwell, 2003; Zhi et al., 2022). An essential piece of evidence is that, statistically, fatigue at the holed parts accounts for 50–90% of aircraft fatigue failures (Liu et al., 2007; Fu et al., 2015); therefore, the fatigue strength of holed segments must be carefully designed and checked.

The experimental investigation on the fatigue strength of holed plates started very early. In 1986, DuQuesnay et al. (1986) performed fatigue tests on the holed plates made from Al 2024-T351 alloy and SAE 1045 steel. However, due to the limitation of the finite element (FE) simulation tool at that moment, no theoretical model was developed except for an empirical relationship between the notch radius and the fatigue notch factor, which cannot provide general guidance for

* Corresponding author. Faculty of Civil Engineering and Geosciences, Delft University of Technology, Delft, 2628 CN, the Netherlands
E-mail address: jacorreia@fe.up.pt (J. Correia).

https://doi.org/10.1016/j.oceaneng.2023.116328
Received 3 July 2023; Received in revised form 27 October 2023; Accepted 11 November 2023
Available online 24 November 2023

Nomenclature

Symbols

$\lg\overline{a_1}$	intercept of lg N axis (in DNV-RP-C203)
b	axial fatigue strength exponent
c	axial fatigue ductility exponent
C_i $(i = 1, 2, 3)$	kinematic hardening moduli i
E	elastic (Young's) modulus
$f(R_\sigma)$	Taras–Greiner stress normalization expression
K'	cyclic strength coefficient
N, N_f	number of cycles to failure
N_c	number of cycles for fatigue strength categorizing
$N_{f,p}$	predicted fatigue life
$N_{f,t}$	tested fatigue life
n'	cyclic strain hardening exponent
P_s	probability of survival
R	notch radius
R_m	tensile (ultimate tensile) strength
R_{mH}	upper yield stress (strength)
R_ε	load strain ratio
R_σ	load stress ratio
S_a	nominal stress amplitude
ΔS	nominal stress range
ΔS_c	nominal stress range at N_c
ΔS_{norm}	normalized nominal stress range
γ_i $(i = 1, 2, 3)$	decreasing rate of kinematic hardening moduli i
ε	strain
ε_a	strain amplitude
$\varepsilon_{a,e}$	elastic strain amplitude
$\varepsilon_{a,p}$	plastic strain amplitude
ε_f'	axial fatigue ductility coefficient
$\varepsilon_{n,a}$	maximum principal strain amplitude
$\Delta\varepsilon_p$	plastic strain range
ν_e	elastic Poisson's ratio
σ	stress
$\sigma_{0.2}$	0.2% offset cyclic yield stress
σ_a	stress amplitude
σ_0	yield surface size
σ_f'	axial fatigue strength coefficient
σ_m	mean stress
$\sigma_{n,max}$	maximum normal stress on the critical plane
$\Delta\sigma$	stress range

Abbreviations

CFRP	carbon fiber reinforced polymer
CMB	Coffin–Manson–Basquin
DNV	Det Norske Veritas
FE	finite element
GFRP	glass fiber reinforced polymer
LVDT	linear variable differential transformer
NBL	label of the hold thick plates after surface processing
OBL	label of the hold thick plates before surface processing
SWT	Smith–Watson–Topper

engineering design. Later, a great deal of work was conducted to build effective methods for accurate fatigue life evaluation of holed components. Experiments have been conducted both in the air (Gong et al., 2002) and other service environments (Liu et al., 2015) to observe fatigue crack initiation and/or propagation behaviours. These studies were combined with macro-microscopic fracture surface analysis to identify damage mechanisms (Gates and Fatemi, 2016; Stawiarski, 2018). Methodologically, various models developed from different perspectives were raised to characterize the notch effect (stress concentration) on fatigue performance. Representative methods include the local stress–strain approaches (Conle and Chu, 1997; De Jesus et al., 2014) (to be combined with some popular multiaxial fatigue models (Mohammadi and Rahmatfam, 2021)), critical distance theory (Susmel and Taylor, 2007), and the highly stressed volume concept (Kuguel, 1961). In addition, for anisotropic materials, the effects of crystallographic orientation should be further considered (Dong et al., 2015).

Recently, with the increasing understanding of the significance of combined notch and size effects modelling in deducing fatigue strength of large-scale engineering components based on fatigue properties derived from small-scale specimen testing (a practical requirement) (Mäde et al., 2018), some improved methods were built. A popular option is the combination of critical distance and highly stressed volume concepts, which has been validated by Wang et al. (2017a) and He et al. (2021). In particular, given the probabilistic aspects of fatigue, Liao et al. (2020b) developed a probabilistic framework for fatigue life assessment of notched components under size effects, whose effectiveness was confirmed by experimental data of central circular holed plate specimens of different scales. Almost instantaneously, a calibrated weakest-link model for probabilistic fatigue assessment was raised by Liu et al. (2020).

In addition to establishing fatigue models of high-precision for structural safe design, some researchers tried to improve the fatigue resistance of holed patterns by altering residual stress distribution. Available techniques include interference fit (Chakherlou et al., 2010), cold expansion (Chakherlou and Vogwell, 2003), laser shock peening (Tan et al., 2004; Cuellar et al., 2012), cavitation peening (Soyama and Takeo, 2016) and shot peening (Esmaeili et al., 2014; Takakuwa et al., 2016) (or double shot peening (Zhi et al., 2022)). Although different post-treatments were utilized, they share a common principle — inhibit or retard crack initiation by generating compressive residual stress on the hole edge. We would also like to highlight the interesting work by Wang et al. (2017b), which explored using carbon fiber reinforced polymer (CFRP) to strengthen the fatigue performance of holed plates.

Based on the literature we collected on fatigue modelling of holed plates, a table of the plate thickness tested before is built, see Table 1. In detail, it is presented in ascending order according to the plate thickness. It's worth noting that the maximum thickness of the plates tested before is only 8 mm, which is much thinner than the downscaled specimen tested in our work (for commercial projects, thicknesses between 100 and 200 mm are foreseen). Besides, most studies were focused on Al 2024-T3, Al 7075-T6 and Ti–6Al–4V (TC4) alloys for aircraft parts where reinforcement techniques can be applied to the holes owing to their higher manufacturing budget and reliability demand compared with other engineering fields.

In fatigue analysis, except for developing models of high precision to correlate fatigue data, the consideration of probabilistic aspects is also a matter of great concern (Socie, 2003). As pointed out by Smith, to perform engineering designs, different from scientific investigations which only care average test data more, extreme test data must be paid attention, see Fig. 1. In particular, there were rich achievements in four aspects of fatigue variability, including fatigue life (Correia et al., 2017; Beretta et al., 2016), fatigue strength (Aigner et al., 2019; Pedrosa et al., 2020), crack growth (Li et al., 2020; Liao et al., 2008) and cumulative damage (Fernández-Canteli et al., 2014; Dias et al., 2019).

Herein, the developing trend of probabilistic fatigue is analyzed based on Web of Science Core Collection (1970–2020), see Fig. 2. In detail, we count the number of publications whose titles with "Probabilistic Fatigue" and "Fatigue", respectively (it is not a rigorous way, but

Table 1
A survey of the plate thickness in existing studies on central holed plate fatigue (mm).

Material	Thickness	Fatigue regime	Reference
Al 2024-T3 alloy	2	Low cycle	Esmaeili et al. (2014)
GFRP composite	2	High cycle	Stawiarski (2018)
Al 2024-T3 alloy	2.28	Low cycle	Mohammadi and Rahmatfam (2021)
Single crystal nickel-base superalloy	2 and 2.5	Low cycle	(Dong et al., 2015; Fan et al., 2022)
Al 2024-T351 alloy and SAE 1045 steel	2.5	High cycle	DuQuesnay et al. (1986)
Al 2024-T3 alloy	3.175	Low cycle and high cycle	Gates and Fatemi (2016)
Ti–6Al–4V alloy	3.81	Low cycle	Cuellar et al. (2012)
A100 steel	4	High cycle	Zhi et al. (2022)
JIS A2017-T3 alloy	4	High cycle	Soyama and Takeo (2016)
Al 7075-T6 alloy	4.5	Low cycle and high cycle	(Chakherlou et al., 2008, 2010)
GH4169 alloy and TA19 alloy	2.4, 3.6, 4.8 and 6	Low cycle	(Wang et al., 2017a; Liu et al., 2020)
En3B steel	6	Medium cycle	Susmel and Taylor (2007)
CFRP strengthened steel	6	High cycle	Wang et al. (2017b)
Al 7075-T6 alloy	6.32	High cycle	Chakherlou and Vogwell (2003)
TC4 alloy	7	High cycle	Liu et al. (2015)
Puddle iron	5, 6, 7 and 8	High cycle	De Jesus et al. (2014)
StE460 steel	40	High cycle	Current work

it doesn't affect drawing a harsh conclusion). Note from the figure, probabilistic issues are receiving increasing popularity in the field of fatigue. However, it still deserves further attention, as until recent years, only about 1% of fatigue relevant literatures take scatter/probability into consideration. To conclude, this is a promising but not yet well discovered subfield. This work will also do probabilistic fatigue analysis.

In modern society, to meet people's aspirations for a better life, larger infrastructures are needed. An example is wind turbines with higher power ratings, which call for advancing methods to ensure their structural integrity (Liao et al., 2022). In a newly developed C1 Wedge Connection for wind turbine assembly (Creusen et al., 2022), a central holed thick plate pattern was included. Through preliminary analyses and tests (Creusen et al., 2022; Cheng et al., 2023a), it was identified as the most fatigue-sensitive detail in the assembly, which will later be shown in Fig. 8. As a result, this work was planned. The three-dimensional view of the scaled central holed thick plate is presented in Fig. 3. As a commercial product, only its length, width and height are given here.

This work aims to develop a general and efficient method for fatigue life prediction of holed thick plates. The rest of the sections are arranged as follows: Section 2, material and structural level tests; Section 3, fatigue data analysis, FE simulation, facture surface observation and fatigue categorizing according to industry codes; Section 4, probabilistic fatigue life prediction; and finally, Conclusions which reports critical findings. Fig. 4 presents the flowchart of this work.

2. Experimental campaigns

2.1. Fatigue test on StE460 steel

The central holed thick plate is made from StE460 steel — a high-strength weldable fine-grain commercial structural steel typically used in bridges, long-span structures, high-rise buildings and other architectural structures. Both uniaxial tension and axial fatigue tests were designed to determine its mechanical and fatigue properties. The geometry and dimensions of the uniaxial tension specimen are plotted in Fig. 5. During the test, strain was measured by an extensometer with a 50 mm gauge length clamped at the middle of the 60 mm parallel portion. The monotonic stress–strain curve is shown in Fig. 6.

The axial fatigue test was performed under strain control mode with symmetric waves, i.e. $R_\varepsilon = -1$, see Table 2. The information about stress and strain was collected at corresponding half-life cycles. The material parameters derived based on the abovementioned tests are tabulated in Table 3, and the relationship between the tested data and the Coffin–Manson–Basquin (CMB) master curve is shown in Fig. 7.

2.2. Fatigue test on the holed thick plate

The equipment for holed thick plate testing is a Schenck® PCX 0001 fatigue test rig with ±600 kN load capacity. Based on the studied object's loading limit and service condition, downscaled experiments with the specimen displayed in Fig. 3 were conducted. For consistency with the boundary condition of the full-scale part, the same assembly mode was used, see Fig. 8. The holed thick plate studied here is the lower

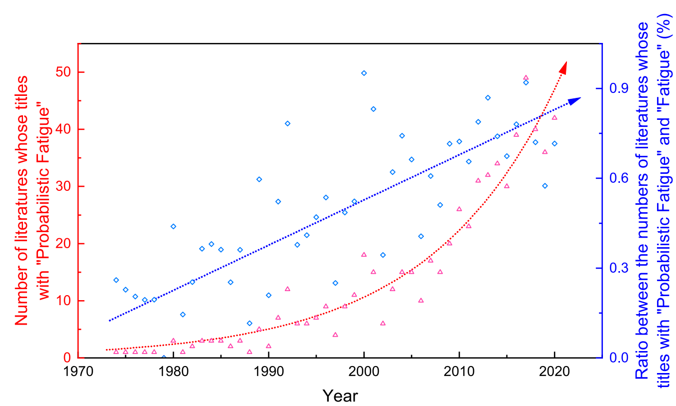

Fig. 2. The developing and promising 'probabilistic fatigue'.

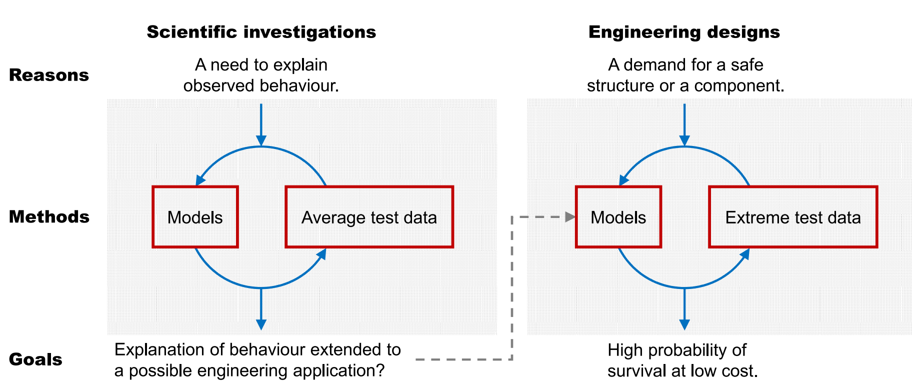

Fig. 1. Differences between scientific investigations and engineering designs in fatigue research (Smith et al., 1986).

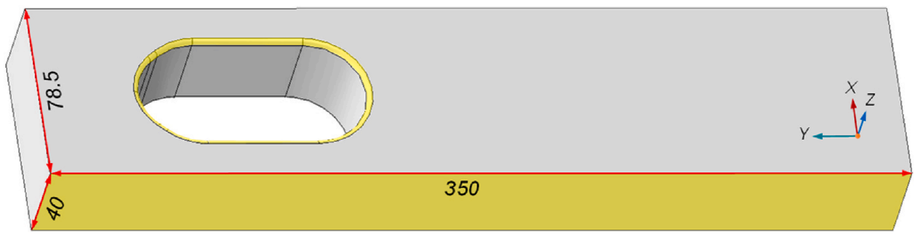

Fig. 3. Three-dimensional view of the central holed thick plate (All dimensions are in mm).

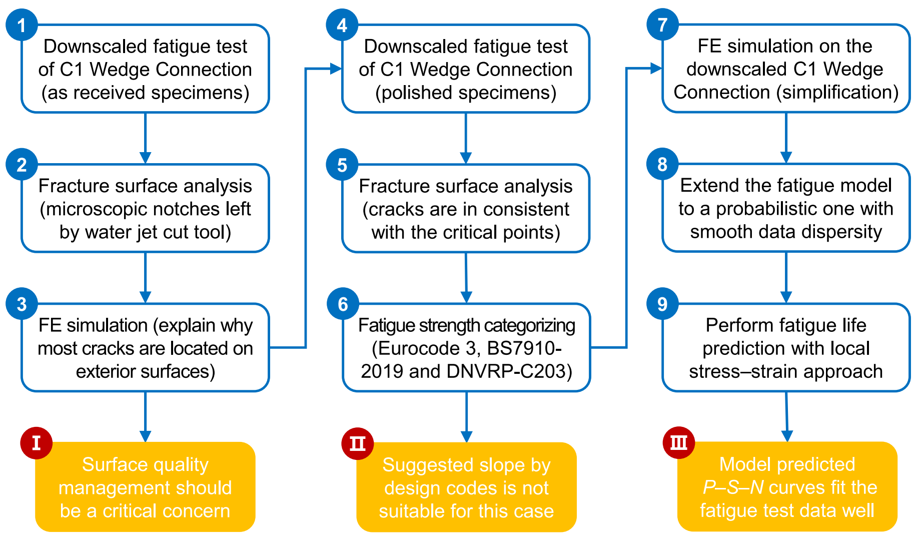

Fig. 4. The flowchart of this work.

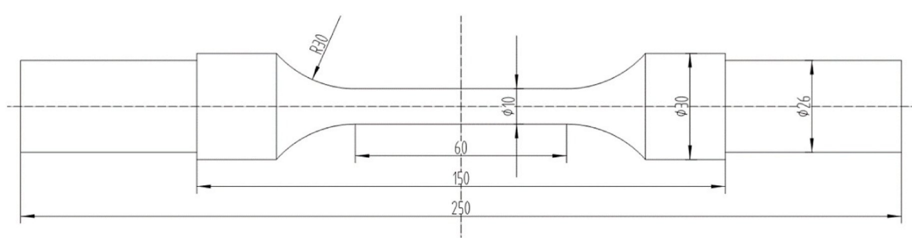

Fig. 5. Geometry and dimensions of the uniaxial tension specimen (mm).

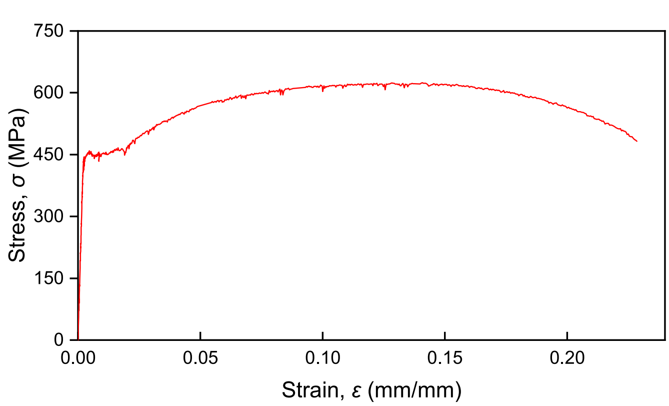

Fig. 6. Monotonic stress–strain curve.

segment in Fig. 8a.

For every specimen, the bottom end in Fig. 8b was clamped at first. Then, when assembling, the pretightening force was applied by a torque wrench on a nut and measured by a load cell, as is presented in Fig. 9. To be more specific, the preload on the bolt of each specimen is 80 kN (measured by torque spanner), and the distributed force transferred to the upper hole edge of the studied object is 405 kN (derived by FE simulation which will be presented later in Section 4). After that, the top end shown in Fig. 8b was directly clamped. The load stress ratio was 0.1 with a sinusoidal loading wave. The load frequency was adjusted to 5 and 12 Hz, respectively, according to the load level. The specimens were tested until failure, and their stiffness degradations were monitored during the tests. A “run out” conclusion will be drawn if a specimen doesn’t fail after at least 3,000,000 cycles (the loaded cycles are not fixed as there are holidays sometimes).

Fatigue test data of holed thick steel plates are presented in Table 4, which includes two sets: OBL and NBL. OBL refers to as machined holed thick steel plates of poor surface quality provided by the manufacturer, while NBL refers to those later carefully polished. Inner means that the crack initiates from the central hole, while exterior indicates the crack starts from one of the two side faces. More details about their difference will be elaborated in Section 3. The failure location was classified according to the subregions marked in Fig. 11. The gross section is 78.5

Table 2
Axial strain-controlled fatigue data.

Stress amplitude, σ_a (MPa)	Mean stress, σ_m (MPa)	Strain amplitude, ε_a (%)	Cycles to failure, N_f (cycle)	Run out
627.4	0	2.00	228	
651.3	0	2.00	250	
544.5	0	1.00	1.240	
551.5	0	1.00	1.295	
450.0	0	0.50	4.340	
450.2	15.6	0.50	6.000	
451.9	3.1	0.50	6.500	
461.1	3.1	0.50	6.600	
466.0	0	0.50	7.450	
377.2	0	0.30	22.000	
392.2	0	0.30	23.000	
378.2	0	0.30	37.580	
383.4	−4	0.30	41.300	
386.0	−2.7	0.30	42.000	
322.3	0	0.20	210.000	
331.2	−7.9	0.20	250.000	
333.8	−9	0.20	250.000	
330.5	−11.5	0.20	254.000	
328.2	21.9	0.20	1.224.800	
332.6	0	0.20	1.750.000	
330.3	0	0.20	2.627.000	
338.8	0	0.20	2.720.000	
329.6	−8.8	0.19	1.000.000	
337.5	−18.5	0.19	23.570.000	Yes
342.8	13.2	0.19	27.470.000	Yes
314.1	0	0.18	532.238	
314.0	0	0.18	1.600.000	
326.4	−22.7	0.18	23.800.000	Yes
324.2	−13.2	0.18	26.100.000	Yes
281.2	0	0.18	99.000.000	Yes
316.9	0	0.18	99.000.000	Yes
303.8	0	0.16	3.420.000	
295.0	0	0.16	99.000.000	Yes
317.3	0	0.16	99.000.000	Yes

Table 3
Mechanical and fatigue properties of StE460 steel.

Parameter	Symbol	Value	Unit
Elastic (Young's) modulus	E	208	GPa
Elastic Poisson's ratio	ν_e	0.29	/
0.2% offset cyclic yield stress	$\sigma_{0.2}$	434	MPa
Tensile (ultimate tensile) strength	R_m	624	MPa
Upper yield stress (strength)	R_{mH}	457	MPa
Cyclic strength coefficient	K'	1181	MPa
Cyclic strain hardening exponent	n'	0.161	/
Axial fatigue strength coefficient	σ_f'	1124	MPa
Axial fatigue ductility coefficient	ε_f'	0.1925	/
Axial fatigue strength exponent	b	−0.094	/
Axial fatigue ductility exponent	c	−0.437	/

mm × 40 mm = 3140 mm^2.

Note from Table 4, there are various load ratios, which need to be unified by mean stress effect models (Pawliczek and Rozumek, 2020). For the convenience of later analyses, a general normalization formula raised by Taras and Greiner for mean stress effect correction was introduced (Taras and Greine, 2010; Pedrosa et al., 2019):

$$\Delta S_{\text{norm}} = \frac{\Delta S}{f(R_\sigma)} \tag{1}$$

where ΔS is the applied nominal stress range, ΔS_{norm} is the normalized nominal stress range, and $f(R_\sigma)$ is the Taras–Greiner stress normalization expression. In particular, for mild steel developed after 1900 (StE460 steel), the normalization expressions are as follows:

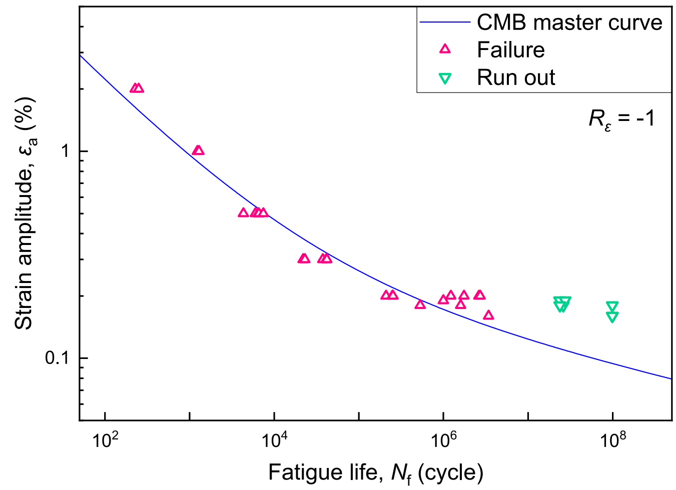

Fig. 7. Fatigue data and CMB master curve.

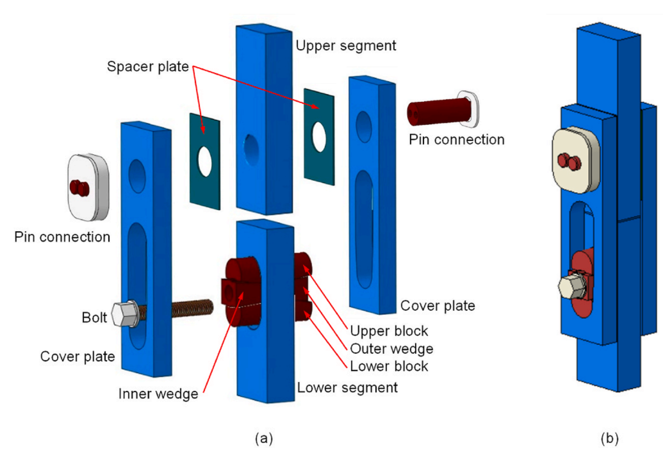

Fig. 8. CAD graphs of the C1 Wedge Connection: left in an explosive view, and right in an assembly view.

$$f(R_\sigma) = \begin{cases} \dfrac{1 - R_\sigma}{1 - 0.4 \times R_\sigma}, (-1 \le R_\sigma \le 0) \\ \dfrac{1 - R_\sigma}{1 - 0.6 \times R_\sigma}, (R_\sigma > 0) \end{cases} \tag{2}$$

The normalized nominal stress range on the gross section ($R_\sigma = 0.1$) is listed in Table 4 as well.

3. Fatigue data analysis of the holed thick plate

3.1. Experimental results before surface polishing

The external surfaces of the segments and plate components shown in Fig. 8 were cut by a water jet tool. As a result, they are relatively rough compared to the machined surfaces on the holes. Initially, 10 OBL specimens (without surface polishing) were tested under several load levels (as shown in Table 4). It was found that the crack sources of 8 out of 10 specimens are located on the exterior surfaces, while in practice, fatigue damage is expected to start from the inner hole edge with higher stress level due to stress concentration (Fig. 18).

The *S–N* plot of the holed thick plate before polishing is depicted in Fig. 10 (note that the lines inside were not fitted by experimental data, but only used to show the tendencies), and a schematic diagram, which includes all crack growth paths, is presented in Fig. 11.

In Fig. 11, only the crack growth paths of eight specimens numbered

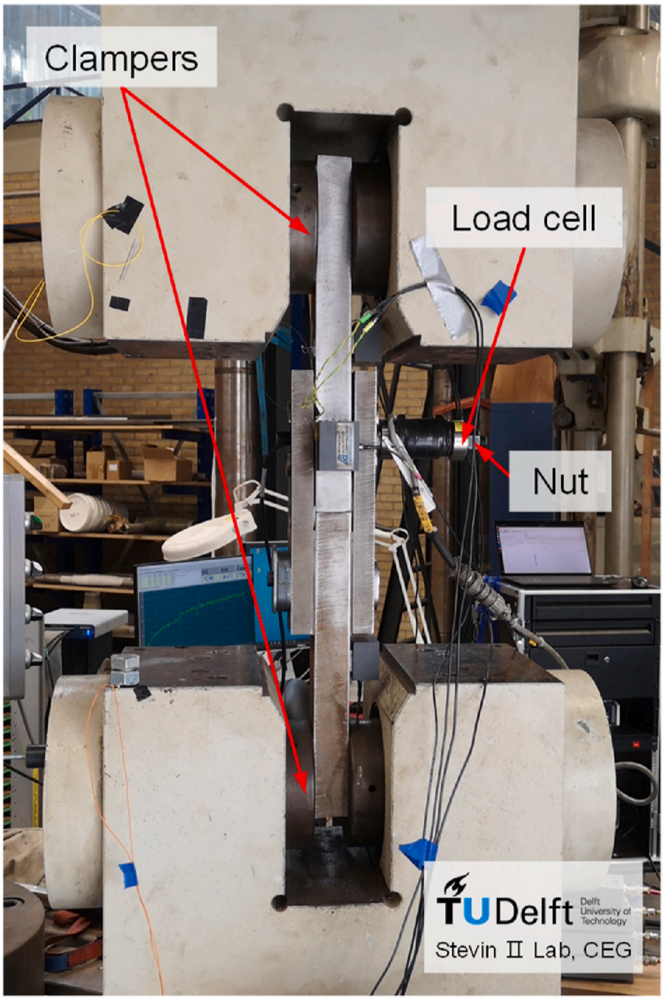

Fig. 9. Experimental setting.

OBL02, and OBL04 to OBL10 are displayed, as the other two were not kept after documenting the failure subregions (Table 4). For specimens OBL02 and OBL08 (see Fig. 12a), their fatigue origins are located in the inner hole edges and are within the middle subregion with a minimum cross-sectional area. This region has both high stress level and high stress gradient (Fig. 18), so cracks are inclined to nucleate (Liao et al., 2020a). Specifically, multi-site crack sources were found, while the lead cracks seat at the chamfering. But why are the crack sources of other specimens all located on the exterior surface?

With this question, we carefully checked the other fracture surfaces and found a potential cause — manufacturing defects of external surfaces. In fatigue analyses, the influence of surface quality-related factors on fatigue strength is called the surface size effect (Kloos, 1976; Singh et al., 2019). For the OBL specimens, apparent micro notches were found everywhere (see Fig. 13), especially on the exterior surface. It is worth noting that the presence of microscopic notches on the exterior surfaces of the specimens was attributed to the draglines of the water jet cut tool. However, such notches will not be present in the standard commercial production of C1 Wedge Connection parts. Fatigue cracks of specimens OBL04, 05, 06, 07, 09 and 10 initiated from their notch roots. For the sake of brevity, only the fracture surfaces of specimens OBL07 (bottom) and OBL09 (top), whose micro notches are more apparent, are presented here (Fig. 12b and c).

Micro notches are visible in the lower right corner of Fig. 12b and the

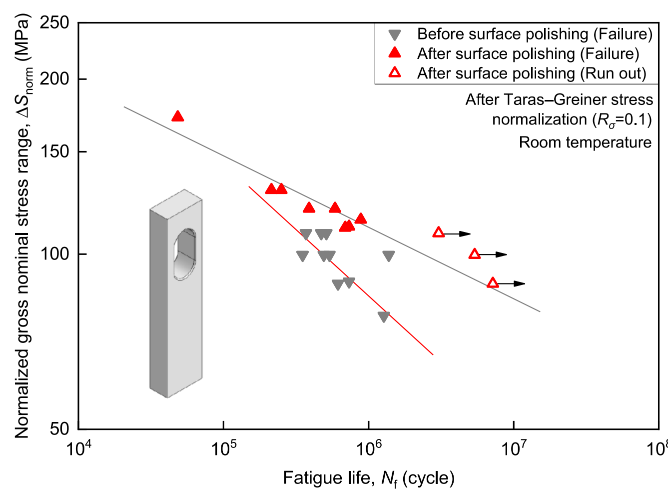

Fig. 10. *S–N* plots of holed thick plates.

Table 4
Fatigue test data of holed thick steel plate.

Specimen No.	Applied load (kN)	Stress ratio	Nominal stress range (gross section, MPa)	Normalized nominal stress range (gross section, MPa, $R_\sigma = 0.1$)	Load frequency (Hz)	Fatigue life (cycles)	Failure subregion	Inner or exterior
OBL01	40–380	0.105	108.28	108.68	5	472.470	Bottom	Exterior
OBL02	40–380	0.105	108.28	108.68	5	511.500	Middle	Inner
OBL03	40–380	0.105	108.28	108.68	5	369.973	Bottom	Exterior
OBL04	40–350	0.114	98.73	99.72	12	537.302	Middle	Exterior
OBL05	40–350	0.114	98.73	99.72	12	1.378.163	Bottom	Exterior
OBL06	40–350	0.114	98.73	99.72	12	350.701	Bottom	Exterior
OBL07	40–350	0.114	98.73	99.72	12	491.824	Bottom	Exterior
OBL08	30–310	0.097	89.17	88.97	12	615.604	Middle	Inner
OBL09	34–314	0.107	89.29	89.73	12	733.307	Top	Exterior
OBL10	45–280	0.160	75.00	78.35	12	1.274.741	Top	Exterior
NBL01	60–600	0.100	171.97	171.97	5	48.439	Middle	Inner
NBL02	45–450	0.100	128.98	128.98	5	250.508	Middle	Inner
NBL03	45–450	0.100	128.98	128.98	5	213.987	Middle	Inner
NBL04	10–405	0.025	125.80	119.73	5	586.318	Middle	Inner
NBL05	10–405	0.025	125.80	119.73	5	388.548	Middle	Inner
NBL06	40–400	0.100	114.65	114.65	5	883.595	Middle	Inner
NBL07	26–384	0.068	114.01	111.54	5	733.019	Bottom	Inner
NBL08	30–384	0.078	112.74	111.07	5	689.213	Top	Inner
NBL09	40–380	0.105	108.28	108.68	5	3.040.206	Run out	
NBL10	40–350	0.114	98.73	99.72	12	5.389.052	Run out	
NBL11	30–310	0.097	89.17	88.97	12	7.189.740	Run out	
NBL12	30–310	0.097	89.17	88.97	12	7.189.740	Run out	

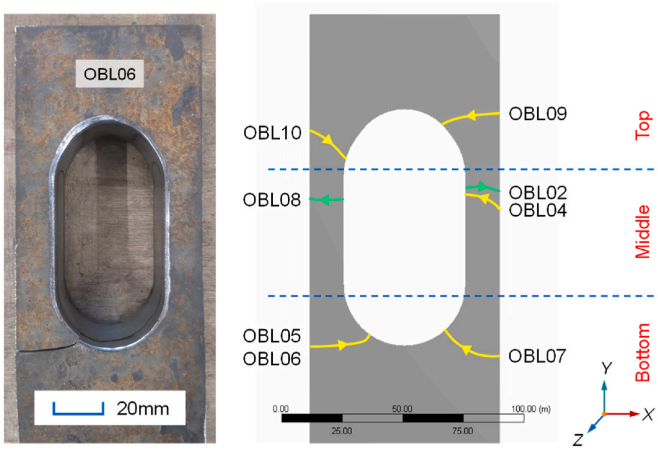

Fig. 11. Crack growth path summary of holed thick plates without surface polishing.

lower left corner of Fig. 12c. The crack sources lie on the notch roots, with all specimens exhibiting multi-site crack initiation. The microcracks are initially located on different material planes. However, with the progressive fatigue damage evolution, they gradually propagated and eventually fused, leaving behind ratchet marks.

3.2. FE simulation with surface defect

It is estimated that the manufacturing defects alter the fatigue crack source locations of holed thick plates from inner holes to exterior surfaces. This subsection tries to verify the surmise made in Subsection 3.1 by FE simulation. To determine the geometrical pattern and dimension of the micro notch for FE modelling, the exterior surfaces of all specimens were scanned with an optical microscope. It was concluded that the notches left by the water jet tool are like sinusoidal waves one after another, and the deepest one is about 350 μm, see Fig. 14.

For simplifying the simulation, a single C shape (semi-circle) notch was built and studied (see Fig. 15a). To study the notch sensitivity (location and size) on local stress distribution, the notch is respectively created at five uniformly-spaced points (Fig. 15b) on the exterior surface. These points cover the crack source locations of tested OBL specimens. Additionally, five notch radii were used in sequence. A two-dimensional model was built for simplification, as stress shows tiny variations along thickness (Wang et al., 2018). The employed FE software is ANSYS® Workbench 19.0. To mitigate the influence of mesh quality, a mesh sensitivity analysis was performed for each model. The mesh refinement was stopped until the relative variation of the maximum principal stress is within 1%.

Considering our focus is the redistributed stress, a unit constant nominal load (net section) was applied in the Y axis direction. The boundary condition is shown in Fig. 15c. The relationship between the maximum stress component along the load direction within the notch region is presented in Fig. 16.

As can be found in Fig. 16, when varying the notch radius from 0.1 to 0.5 mm, the maximum stress components along the load direction show tiny variations. This is likely due to the small dimensions of the notch compared with those of the holed thick plate. However, the stress levels at locations A and E are much higher than the other three locations. Global and local stress distributions at these two locations are shown in Fig. 17.

What's interesting is that positions with high stress levels at locations A and E align with the sites of crack initiations in specimens OBL05, 06, 07, 09 and 10. Of course, crack nucleation can also happen at other locations of the exterior surface if there are better microstructural environments (like specimen OBL4) for crack nucleation. Fig. 18 displays the stress distribution on the exterior surface along the path (from points 1 to 2) for the case without a micro notch.

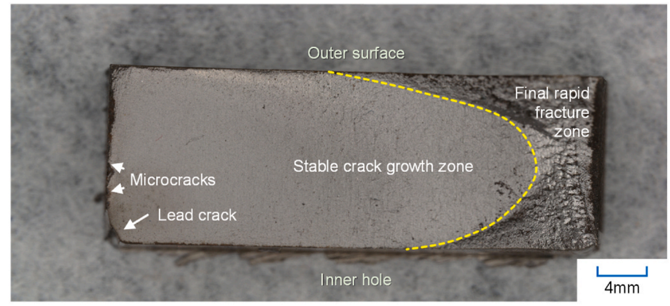

(a) OBL08: 30–310 kN, 12 Hz, 615,604 cycles

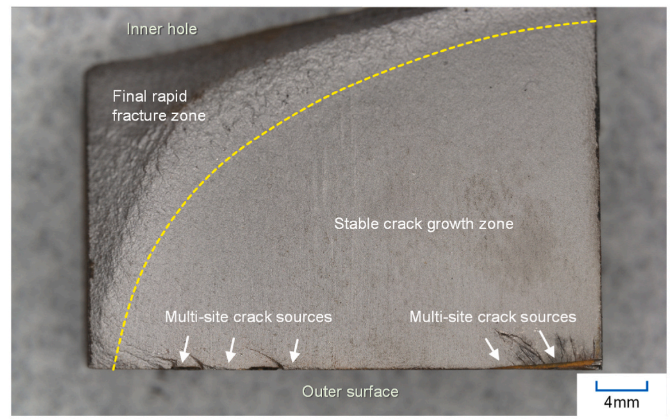

(b) OBL07: 40–350 kN, 12 Hz, 491,824 cycles

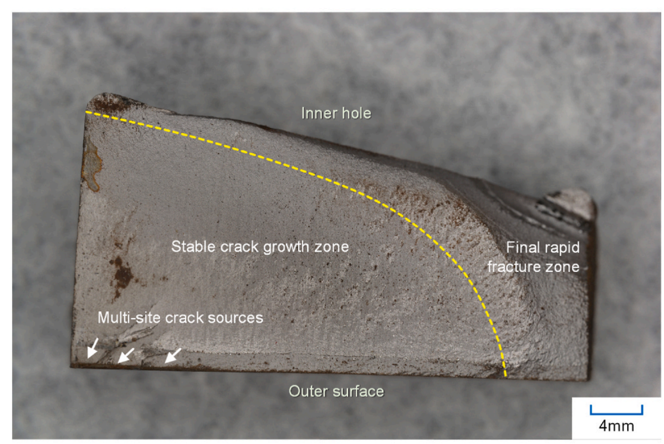

(c) OBL09: 34–314 kN, 12 Hz, 733,307 cycles

Fig. 12. Fracture surfaces of holed thick plates without surface polishing.

Note from Fig. 18, there are two extremes with significantly higher stress levels (very close to points A and E in Fig. 15b). Although, in Fig. 18, the critical point of the highest stress is located in the inner hole edge; if there is a notch on the exterior surface, under the joint effect of initial inhomogeneous stress distribution and additional stress concentration, the critical point will shift to the exterior surfaces (Fig. 17). Therefore, most of the crack sources of OBL specimens are located on the exterior surfaces, especially close to those two extreme points. It should be clarified that the FE simulation on the holed thick plate with a surface defect conducted here is not a quantitative but a qualitative analysis; accordingly, some simplifications were made. However, it is essential to note that the experimental and simulated results of OBL specimens emphasize the significance of surface quality control in manufacturing and the surface size effect on fatigue performance (Suraratchai et al.,

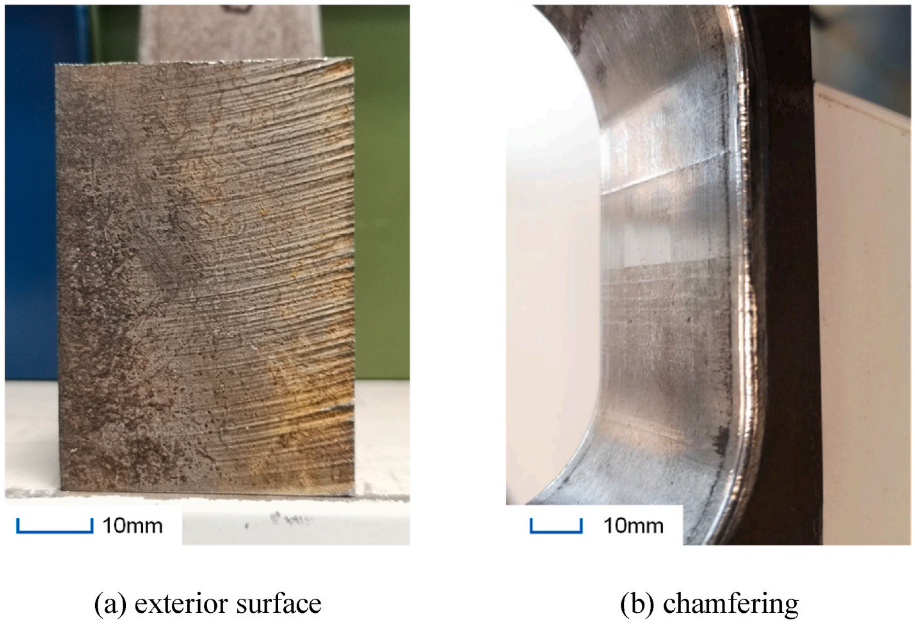

Fig. 13. Manufacturing defects on the as machined holed thick plate.

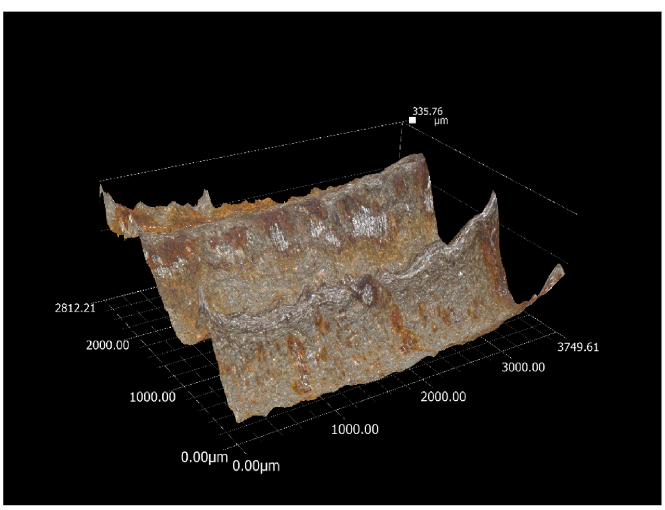

Fig. 14. Micro notch observation on the exterior surface (OBL07).

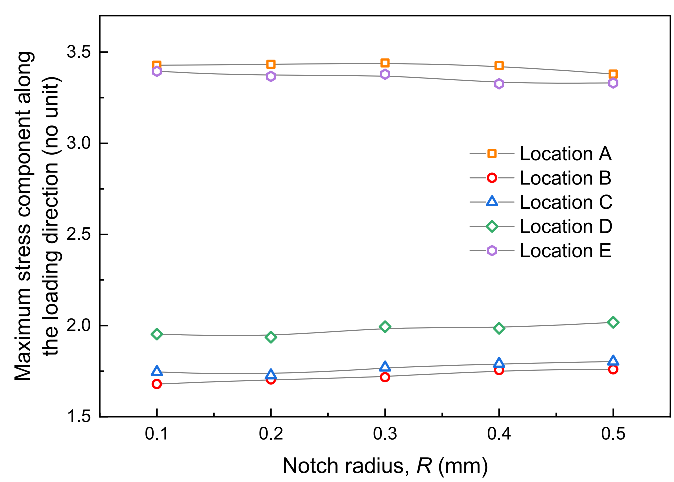

Fig. 16. Maximum notch stress in different locations and sizes.

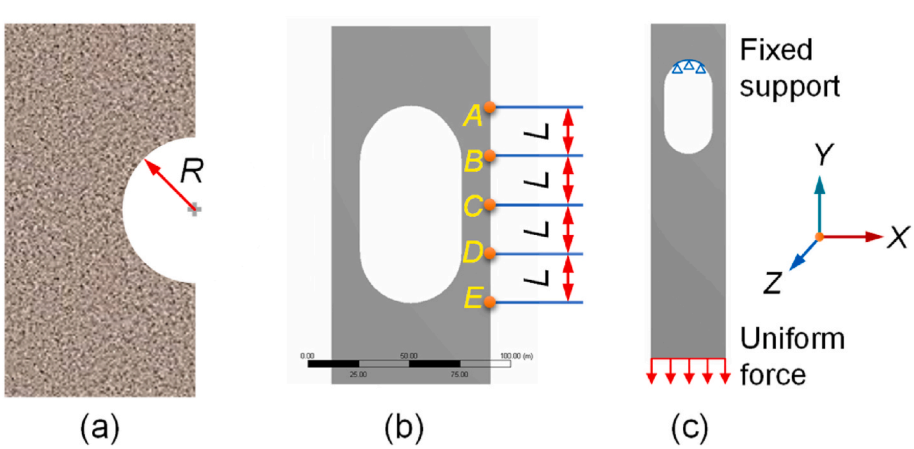

Fig. 15. Details about surface defect (micro notch) simulation.

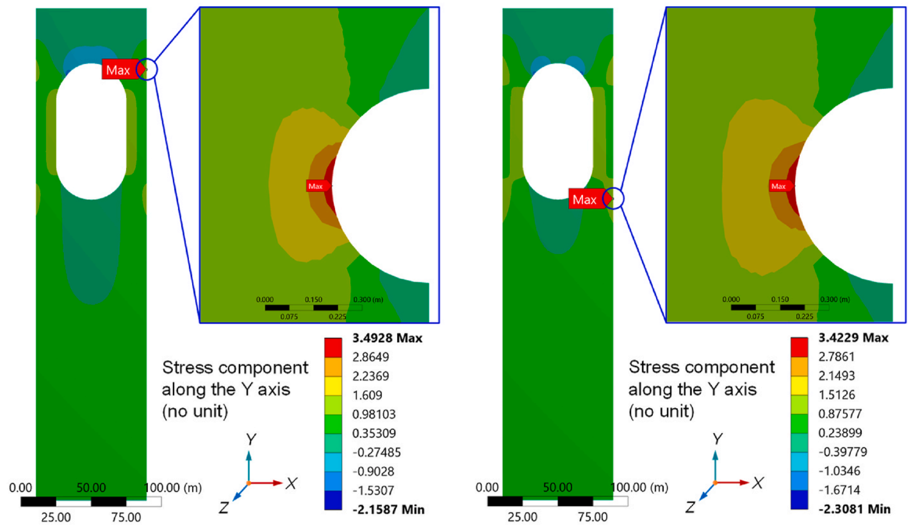

(a) location A, notch radius=0.3 mm (b) location E, notch radius=0.3 mm

Fig. 17. Distributions of the maximum stress component along the load direction.

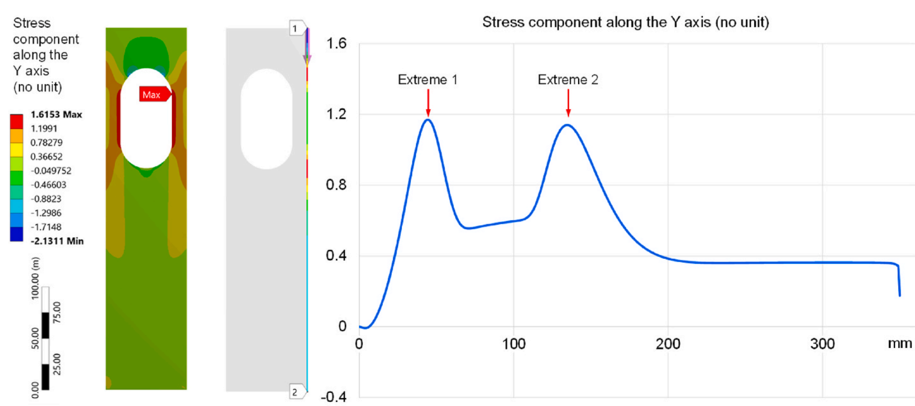

Fig. 18. Stress distribution along the path (from point 1 to 2) without any micro notch.

2008).

3.3. Experimental results after surface polishing

To minimize the effect of the manufacturing defects and chamfering (Fig. 13) to fatigue strength of the holed thick plate, those regions were carefully polished with sandpapers of different grits (firstly 80, then 150 and finally 240) successively. The further polished areas are marked with yellow in Fig. 3. In particular, polishing was performed along the Y axis (the loading direction). Later, 12 specimens after surface polishing (NBL01 to NBL12) were tested.

The fatigue results of NBL specimens are plotted in Fig. 10 as well for comparison. As expected, the further polished specimens show higher fatigue performance than the as machined ones. Particularly, all of the crack sources are located at the inner hole edges within the middle region with higher stress levels (Fig. 18), see Fig. 19. Two representative fracture surfaces are shown in Fig. 20.

Through the fracture surface in Fig. 20 (including Fig. 12), ductile fracture mode can be identified, characterized by extensive plastic deformation. The story goes like this: fatigue crack nucleates at the surface and then propagates into the body; with the progressive fatigue damage process, the cross section gets smaller which leads to higher stress level; finally, when the stress level on the cross section exceeds the

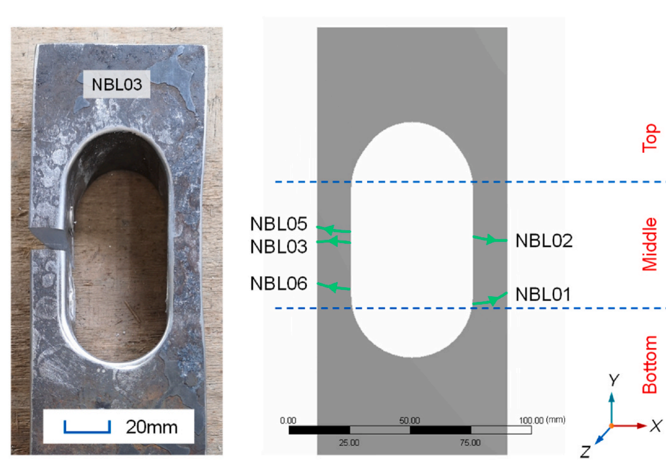

Fig. 19. Crack growth path summary of fractured holed thick plates after surface polishing.

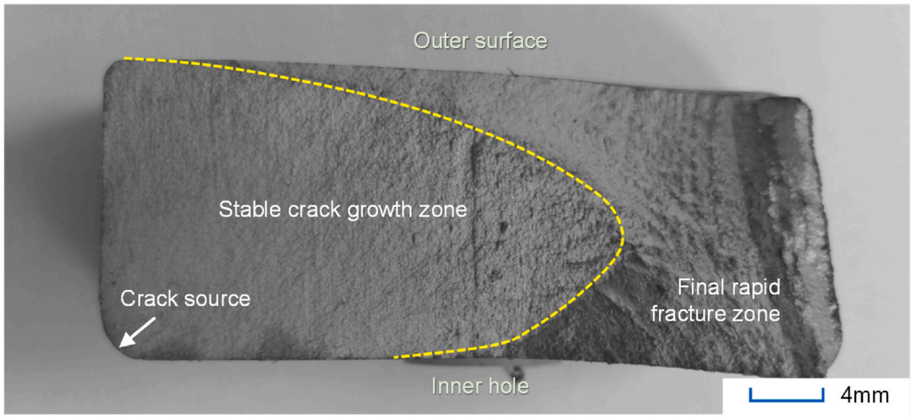

(a) NBL03: 45–450 kN, 5 Hz, 213,987 cycles

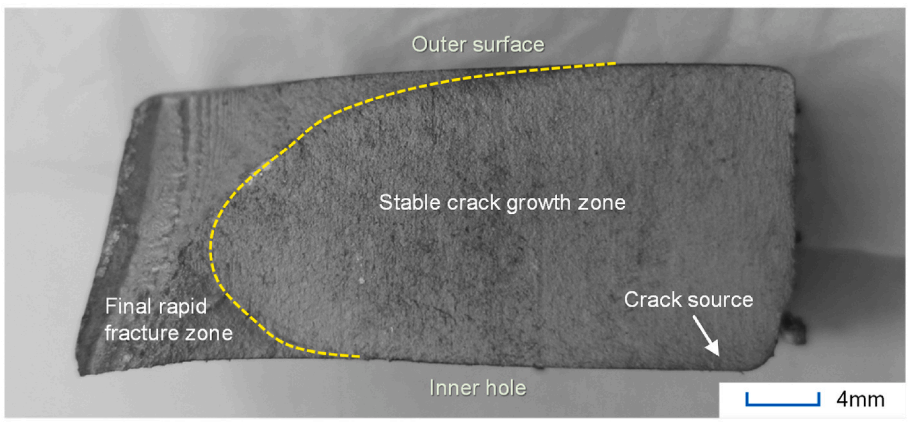

(b) NBL06: 40–400 kN, 5 Hz, 833,595 cycles

Fig. 20. Fracture surfaces of holed thick plates after surface polishing.

material's ultimate limit, ductile fracture happens.

Herein, we would also like to report the results of a fatigue experiment on GH4169 V-notched round bar specimens conducted before at the University of Electronic Science and Technology of China, although it is not a holed plate. When manufacturing the notches, two kinds of techniques were used, i.e. (a) lathe processing, and (b) lathe processing + precision grinding. The tests were carried out under stress-controlled mode with symmetric triangular wave loadings.

Note from Fig. 21, the specimens whose V-notches were further processed by precision grinding show higher fatigue resistance. The significant difference can be explained by diverse V-notch surface quality, see Fig. 22. There are visible micro notches on those specimens machined by lathe processing only, which cause stress concentration and trigger crack nucleation; in contrast, for those further processed by precision grinding, under the same magnification, the surface is flatter.

So, in short, whatever in material testing or engineering production, the surface quality must be adequately controlled to avoid the surface size effect on fatigue behaviour (Suhr et al., 1986).

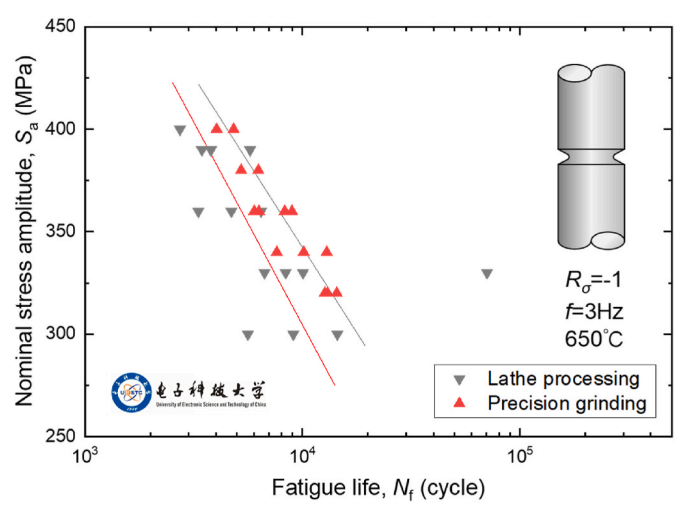

Fig. 21. Fatigue performances of GH4169 V-notched specimens processed by different techniques.

3.4. Categorizing according to industry codes

In the steel structure design, industry codes are commonly utilized to classify fatigue performance. Herein, the widely used European standard (Eurocode 3, Part 1–9) (European Committee for Standardization, 2005), British standard (BS7910-2019) (British Standards Institution, 2019), as well as DNV industry code (DNV-RP-C203) (Det Norske Veritas, 2014) were employed in this research. Despite some differences, for fatigue lives ranging from 10^4 to 10^7 cycles, they share the equation:

$$(\Delta S)^3 N_f = \text{constan t} \tag{3}$$

where N_f is the number of cycles to failure. In other words, the slope of S–N curves are the same, i.e. $-1/3$. Finally, the determined fatigue strength categories based on the abovementioned codes are given in

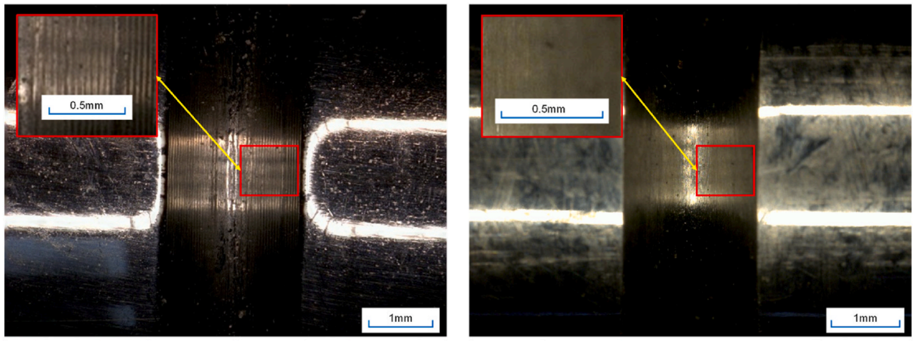

(a) lathe processing (b) precision grinding

Fig. 22. V-notch surface images.

Table 5. In particular, the results derived by Eurocode 3 and BS7910-2019 are presented with ΔS_c — the nominal stress range at the number of cycles for fatigue strength categorizing, N_c; while the results computed according to DNV-RP-C203 are shown in $\lg\overline{a_1}$ — the intercept of $\lg N$ axis.

Table 5 was derived as follows: (a) Linear fit the fatigue results with the given slope (fitted category) based on the least squares estimation method. Although these codes use different categorizing cycles, they share an identical slope of $-1/3$. So, this step receives a single *S–N* curve. (b) Shift category according to the demanded survival probability. (c) Adjust category based on small sample consideration. For BS7910-2019, the final category was taken as the shifted category as no requirement is mentioned; in contrast, for Eurocode 3 and DNV-RP-C203, the final category is the adjusted result with a small sample consideration. During categorizing, only the failed NBL points were included. In particular, the NBL01 point was excluded (the point marked with a blue circle), as it is far away from the majority, and there is no duplicate test. However, it is included in Section 4 where fatigue life prediction is performed.

To conclude, Eurocode 3 suggests a 75% confidence level of 95% survival probability, BS7910-2019 recommends a 97.7% survival limit, and DNV-RP-C203 looks for the *S–N* curves associated with a 97.7% survival probability. More details about the processes can be found in the corresponding code. The final categories are plotted in Fig. 23. Nearby categories are presented as references for comparison purposes. Note from the figures, for NBL data, $m = 3$ cannot reasonably characterize its *S–N* relationship.

Table 5
Fatigue strength categorizing of NBL specimens according to industry codes (MPa).

Standard	Eurocode 3 (European Committee for Standardization, 2005)	BS7910-2019 (British Standards Institution, 2019)	DNV-RP-C203 (Det Norske Veritas, 2014)
Categorizing cycle	$N_c = 2 \times 10^6$ cycles	$N_c = 2 \times 10^6$ cycles	$N_c = 10^7$ cycles
Fitted category	$\Delta S_c = 73.73$ $P_s = 50\%$	$\Delta S_c = 73.73$ $P_s = 50\%$	$\lg\overline{a_1} = 11.90$ $P_s = 50\%$
Shifted category	$\Delta S_c = 59.61$ $P_s = 95\%$	$\Delta S_c = 56.98$ $P_s = 97.7\%$	$\lg\overline{a_1} = 11.57$ $P_s = 97.7\%$
Small sample consideration	$\Delta S_c = 57.96$ $P_s = 95\%$	Not mentioned	$\lg\overline{a_1} = 11.52$ $P_s = 97.7\%$
Final category	$\Delta S_c = 57.96$ $P_s = 95\%$	$\Delta S_c = 56.98$ $P_s = 97.7\%$	$\lg\overline{a_1} = 11.52$ $P_s = 97.7\%$
Nearby category	$\Delta S_c = 56$	Q5 ($\Delta S_c = 50$)	G ($\lg\overline{a_1} = 11.40$)

4. Probabilistic fatigue life modelling

This section introduces a new method for probabilistic fatigue modelling and its application on a holed thick steel plate. First, two alternative models for later analysis were presented and validated with experimental results of the smooth specimens. Then, in light of the dispersity of fatigue data, a method to generate scatter bands was proposed, which shows favourable performance. Finally, the *S–N* curves of the holed thick steel plate were obtained with the abovementioned models based on the stress–strain derived by FE simulation under the same load conditions as experiments.

4.1. Fatigue models

Given the tensile dominant stress state of the studied object as well as the material level fatigue data in Table 2, the CMB (American Society for Testing and Materials, 2012) and the Smith–Watson–Topper (SWT) (Smith et al., 1970) models were introduced.

CMB model:

$$\varepsilon_a = \varepsilon_{a,e} + \varepsilon_{a,p} = \frac{\sigma_f^{'}}{E}(2N_f)^b + \varepsilon_f^{'}(2N_f)^c \tag{4}$$

where $\varepsilon_{a,e}$ and $\varepsilon_{a,p}$ are respectively elastic and plastic strain amplitudes.

SWT model:

$$\varepsilon_{n,a}\sigma_{n,\max} = \frac{\left(\sigma_f^{'}\right)^2}{E}(2N_f)^{2b} + \varepsilon_f^{'}\sigma_f^{'}(2N_f)^{b+c} \tag{5}$$

where $\sigma_{n,\max}$ is the maximum normal stress on the critical plane with maximum principal strain amplitude $\varepsilon_{n,a}$ over a stabilized cycle (here, the half-life cycles were utilized). Compared with the CMB model, the SWT model can further consider the mean stress effect. In particular, as a critical plane-based multiaxial fatigue model, it can characterize the non-proportional strengthening effect and predict both fatigue crack initiation cycles and planes (Liao and Zhu, 2019).

To validate the effectiveness of these two models, the material fatigue data were used for validation, see Fig. 24. Note that within 10^2 to 10^6 cycles, they both provide promising predictions, and almost all data points fall within the double scatter bands; however, for those specimens last more than 10^6 cycles, both of them fails to depict the tendency. In particular, these figures present significant data scatter, underscoring the significance of considering the probabilistic aspects of fatigue.

Considering that CMB and SWT models provide accurate prediction from 10^2 to 10^6 cycles and most of the central holed thick plate fatigue data in Table 4 fail within 10^5 to 10^6 cycles, they were employed for later fatigue life prediction.

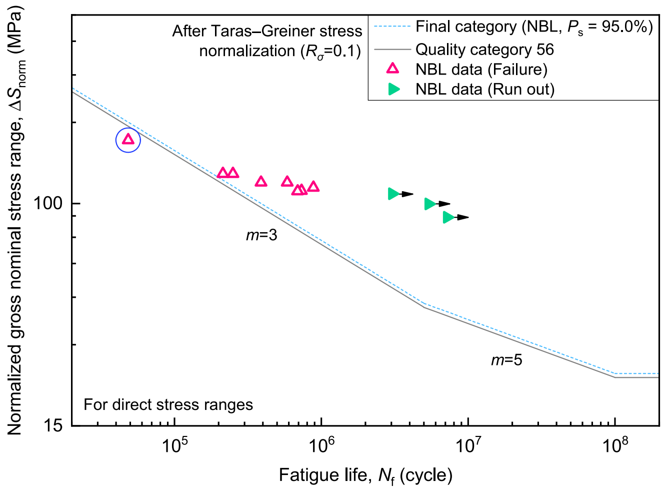

(a) Eurocode 3 [55]

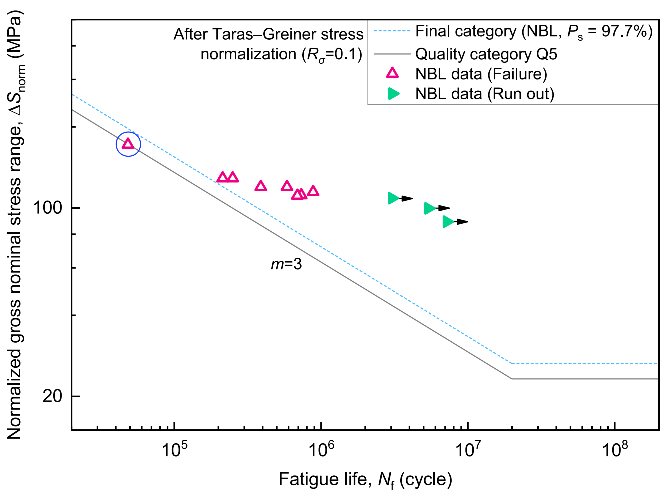

(b) BS7910-2019 [56]

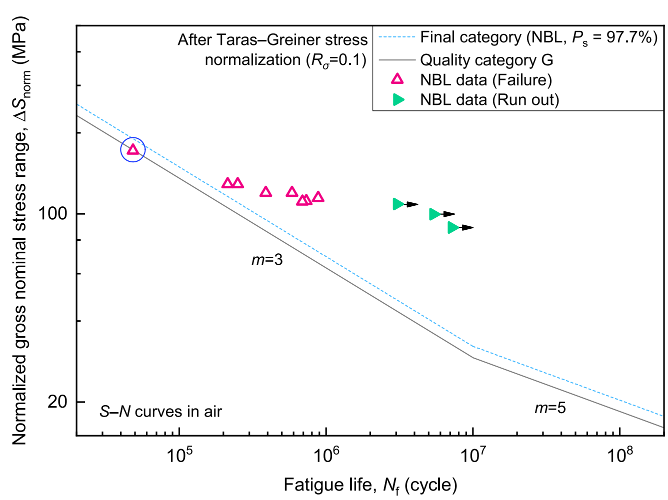

(c) DNV-RP-C203 [57]

Fig. 23. Fatigue strength curves based on different industry codes.

4.2. Probabilistic perspective

With the increasing attention on service reliability of engineering components, probabilistic modelling is now a hot topic in fatigue study (Haldar and Mahadevan, 1999; Schijve, 2009a; Zhu et al., 2017). In particular, sources for fatigue life dispersion of structures come from the following aspects: material property and microstructural feature (Liang et al., 2022), geometry and scale (Niu et al., 2021), manufacturing and processing (Feng et al., 2021), assembly and installation (Li et al., 2022), as well as load and environment (Su et al., 2018).

However, it is hard to cover all potential sources of fatigue data scatter in practical engineering. For this work, as the only source for probabilistic modelling is the fatigue results in Table 2, only the material variability was considered. Specifically, the logarithm fatigue life at each load level was assumed to follow a normal distribution; as a result, deterministic models can be extended to probabilistic ones. Actually, at different load levels, the fatigue lives have diverse standard deviations (Schijve, 2009b); nevertheless, the data in Table 2 is not enough to summarize a rule. So, the standard deviation was assumed to be a constant. Then, the standard deviations of predicting errors using CMB and SWT models were obtained by analyzing $\lg(N_{f,t}) - \lg(N_{f,p})$, which are 0.348 and 0.379, respectively.

The probabilistic analysis results are visible in Fig. 25, together with lower and upper boundaries. Note that for both CMB and SWT models, the scatter bands obtained by the proposed way encircle most failed points; as a result, it was adopted in later probabilistic fatigue life prediction.

4.3. FE simulation and life prediction

According to the experimental settings shown in Fig. 9, the same boundary and load conditions were applied to derive the cyclic stress–strain responses of the holed thick steel plates as inputs for later fatigue life prediction. Under the premise of not changing the load condition of the central holed thick plate, compared with the assembly presented in Fig. 8, only the studied object as well as the simplified lower segment and upper block were created, see Fig. 26. In addition, regarding the symmetry, a 1/4 model was built to enhance computing efficiency (all areas located on XOY and YOZ planes are symmetry planes). Detailed boundary conditions are marked in Fig. 26.

For the lower segment, the material is StE460 steel; while for the upper block, the material is StE620 steel with 210 GPa Young's modulus and 0.3 elastic Poisson's ratio. The transferred preload from the bolt applied to the upper block was obtained by FE simulation on the whole assembly (see Fig. 9) (Cheng et al., 2023a, 2023b), using the same bolt pretension force as applied in the experimental campaign.

Here, ANSYS® Mechanical 19.0 FE software was used. To ensure computational accuracy, 2-order 20-node quadratic brick 3D element Solid 186 was utilized, and the same mesh sensitivity analysis process mentioned in Subsection 3.2 was carried out. The three-term back stress Chaboche model was adopted for constitutive modelling, and the related parameters were determined according to the instruction in (Basan et al., 2017) based on the Ramberg–Osgood model parameters given in Table 3.

$$\frac{\Delta\sigma}{2} = \sigma_0 + \sum_{i=1}^{3} \frac{C_i}{\gamma_i} \tanh\left(\gamma_i \frac{\Delta\varepsilon_p}{2}\right) \tag{6}$$

where $\Delta\sigma$ is the stress range, σ_0 is the yield surface size, C_i (i= 1, 2, 3) are the kinematic hardening moduli, γ_i (i= 1, 2, 3) are the decreasing rates of corresponding kinematic hardening moduli, $\Delta\varepsilon_p$ is the plastic strain range.

When applying the cyclic loading, according to Table 4, 11 load levels (maximum gross nominal stress ranging from 90 to 190 MPa, in arithmetic sequence) were simulated. The load ratio was defined as 0.1. Finally, it was found that the critical point with the maximum stress

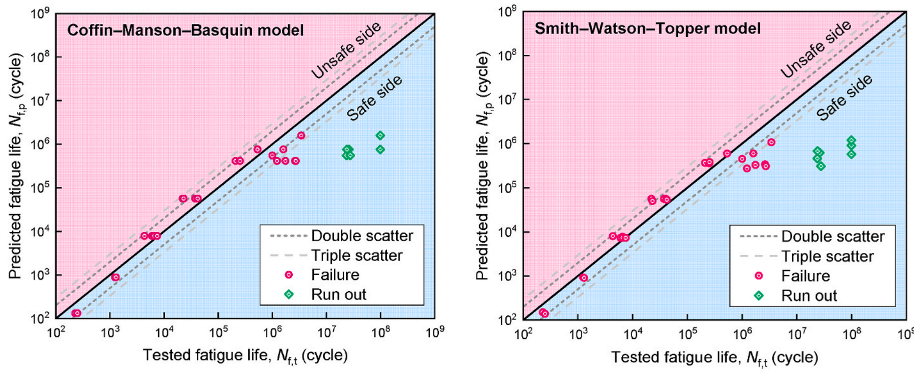

(a) CMB model (b) SWT model

Fig. 24. Predicted versus tested fatigue lives.

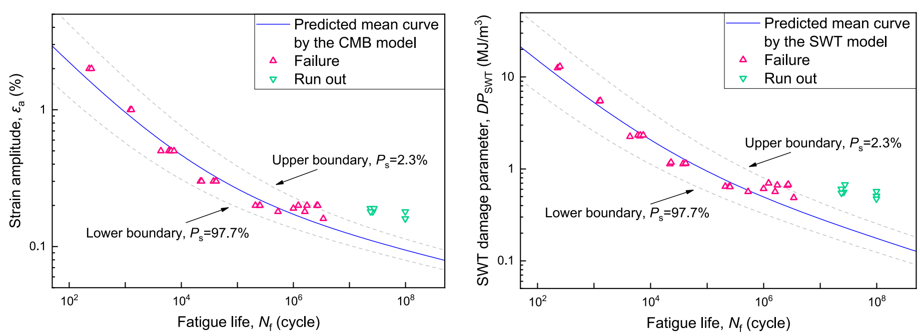

(a) CMB model (b) SWT model

Fig. 25. Probabilistic fatigue modelling (material tests).

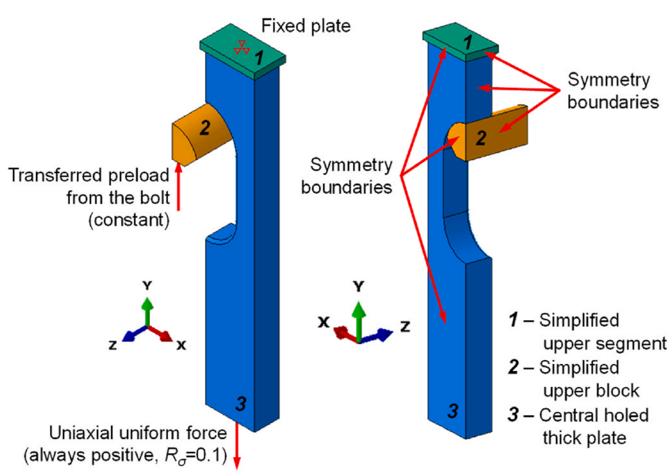

Fig. 26. Boundary and load conditions in FE simulation.

(both the maximum principal stress and the stress component along the Y axis) is always located at the upper edge of the central hole (on the symmetric plane), see Fig. 27.

Actually, in this work, the critical point was not defined by stress nephograms; instead, the points with the maximum damage parameters (the left parts of Eqs. (4) and (5)) among the whole part were chosen, respectively. Eventually, it was found that for both CMB and SWT models, the critical point is the same as the one shown in Fig. 27.

Considering that the initial phase of fatigue damage is a microscopic local phenomenon (Schijve, 1979; Sanaei and Fatemi, 2021) and the scale of the studied object is large comparatively, the local stress–strain approach (Visvanatha et al., 2000; Chen et al., 2014) was utilized for fatigue crack initiation prediction. The stress–strain responses at the critical points were inputted into CMB and SWT models.

In addition, to monitor the fatigue damage evolution process, two linear variable differential transformers (LVDTs) were set on two exterior surfaces of the holed steel thick plate, see Fig. 28a. LVDT No. 1 can be found in the figure, while LVDT No. 2 is arranged on the other side. The measurement range covers points A to E in Fig. 15b, between which fatigue cracks are of high potential to initiate. Through the outputted stiffness variations, it can be concluded that the unstable crack growth phase only takes nearly 10% of the total fatigue life. Accordingly, the fatigue initiation cycles given by CMB and SWT models were roughly adopted as the predicted total fatigue lives of the holed thick plates.

By connecting the predicted lives under 11 load levels, mean curves provided by CMB and SWT models were derived, see Fig. 29. The predicted *S–N* relationships can be fitted with straight lines in a double logarithmic chart. The goodness of fit for the CMB model case is 0.9775, and for the SWT model case is 0.9883. Then, the lower and upper boundaries were obtained by using the standard deviations derived from material tests in Subsection 4.2.

As shown in Fig. 29, for the failed NBL specimens, the SWT model reasonably predicts their fatigue lives, while the CMB model provides too optimistic predictions. This may be attributed to the shortcomings of the CMB model in multiaxial fatigue modelling and mean stress effect correction (You and Lee, 1996; Lukáš and Kunz, 1989). The final category given by the DNV code in Subsection 3.4 is also plotted here for comparison. Comparatively, the slope given by the proposed model (based on the SWT model) works better, which may attribute to a stronger correlation with failure mode; while for the slope suggested by the DNV code, it is after all a general recommendation, so it behaves not so satisfactory. As for the run out NBL specimens, although they are

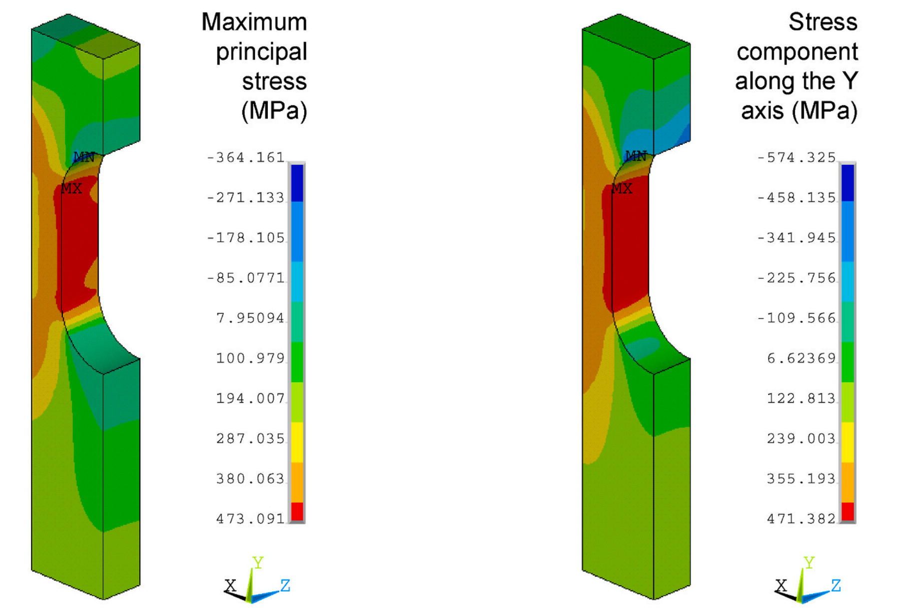

(a) maximum principal stress (b) stress component along the Y axis

Fig. 27. Stress distributions at the load peak substep (140 MPa gross nominal stress).

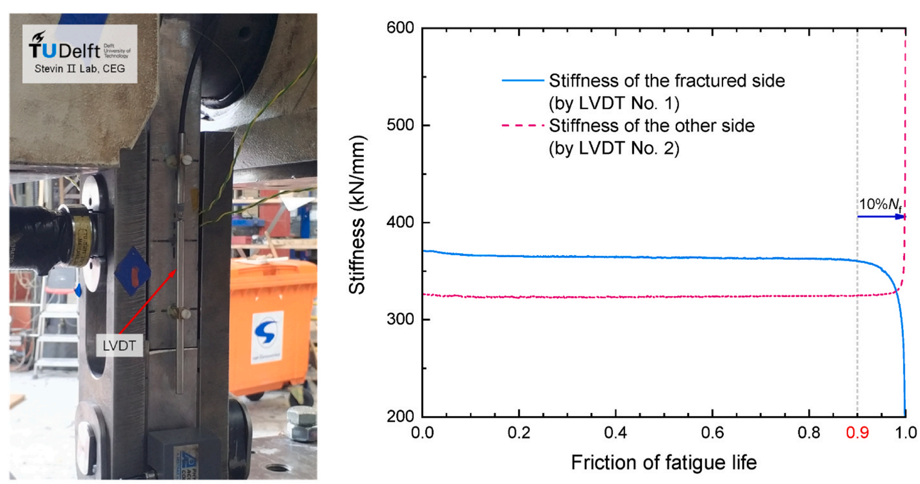

(a) LVDT setting (b) stiffness versus life friction

Fig. 28. Stiffness plot during the test (NBL02).

located within the scatter bands given by the SWT model-based probabilistic model, their total fatigue lives are unknown; so, we didn't do further analysis. Moreover, note from Fig. 25, when $N_f > 5 \times 10^6$ cycles, the predicting errors given by both SWT and CMB models get higher. As a result, it is unclear whether the model is applicable when $N_f > 10^6$ cycles.

5. Conclusions

In this work, a central holed thick steel plate was cyclically tested. Accordingly, facture surface analysis, FE simulation, fatigue strength categorizing and fatigue life prediction were conducted successively, which intends to provide a general solution for fatigue performance assessment of holed thick plates. Major conclusions are drawn as follows.

(1) Surface quality management should be a critical concern in both material fatigue testing and structural strength design, in view of the surface size effect on fatigue behaviour illustrated by fatigue tests of StE460 holed thick plates and GH4169 V-notched round bar specimens.
(2) The slope, $m = 3$, suggested by industry codes (including Eurocode 3, BS7910-2019 and DNV-RP-C203) is not suitable for describing the S–N relationship of the holed thick plate after surface polishing (NBL specimens) tested in this work.
(3) The proposed probabilistic fatigue model based on the SWT model provides a favourable prediction on the S–N relationship of failed NBL specimens, potentially for a stronger correlation with failure mode. In addition, using the local stress–strain approach is acceptable in this case, as crack initiation is a local phenomenon compared to the dimension of the studied object. All of the tested points fall within the lower and upper boundaries corresponding to 97.7% and 2.3% failure probabilities.

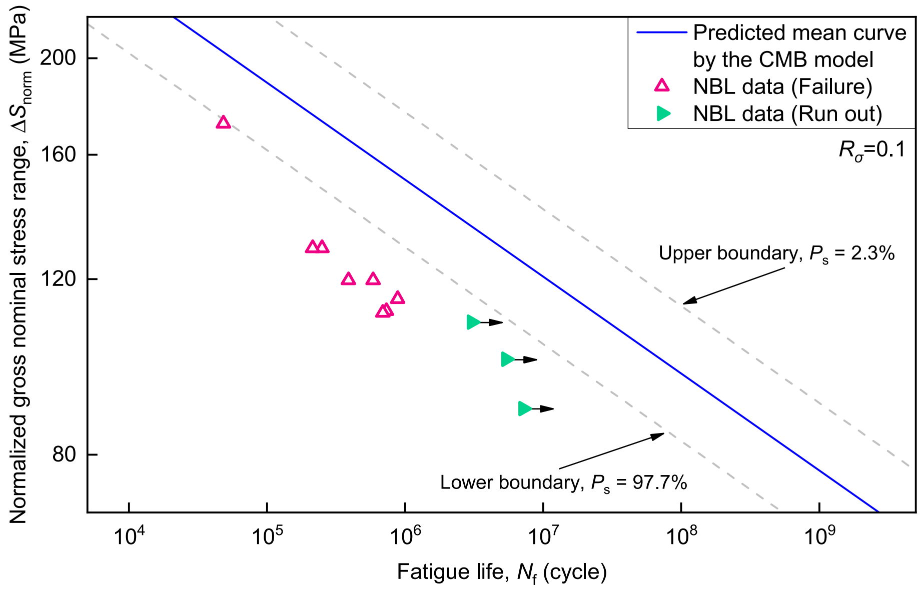

(a) CMB model-based

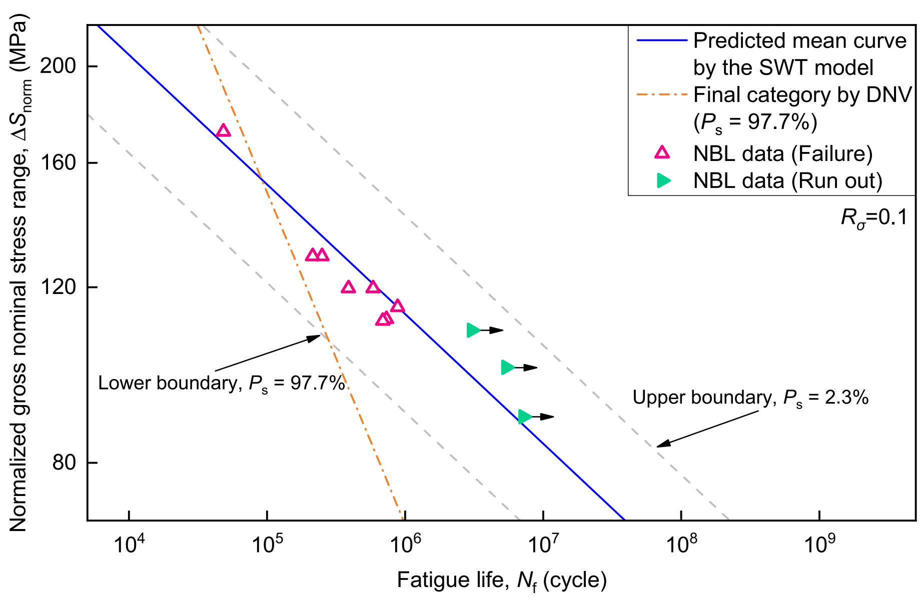

(b) SWT model-based

Fig. 29. Predicted *P–S–N* curves of NBL specimens.

(4) Although it shows an excellent correlation between the predicted *P–S–N* curves and tested data, we used, after all, the local stress–strain approach. But, in this case, as is shown in Fig. 11, the cracks on the lower segment actually initiate from scattering sites. As a result, it would be a promising work to build global damage model for integrating fatigue failure probabilities of all material elements.

CRediT authorship contribution statement

Ding Liao: Investigation, Formal analysis, Writing – original draft, Validation. **Lu Cheng:** Investigation, Formal analysis, Writing – review & editing. **José Correia:** Formal analysis, Writing – review & editing, Supervision. **Milan Veljkovic:** Formal analysis, Validation, Writing – review & editing, Supervision. **Shun-Peng Zhu:** Formal analysis, Writing – review & editing. **Jasper Winkes:** Formal analysis, Validation, Writing – review & editing. **Koen Creusen:** Formal analysis, Validation, Writing – review & editing. **Filippo Berto:** Conceptualization, Writing – review & editing.

Declaration of competing interest

The authors declared that they do not have any commercial or associative interest that represents a conflict of interest in connection with the work submitted, entitled "*Probabilistic fatigue analysis on a central holed thick steel plate of C1 Wedge Connection for wind turbine tower assembling*".

Data availability

The data that has been used is confidential.

Acknowledgement

The authors would like to acknowledge the Delft University of Technology (TUDelft) and C1 Connections for all necessary conditions that allowed the completion of this work. This research was supported by the following grants: base funding - UIDB/04708/2020 and programmatic funding - UIDP/04708/2020 of the CONSTRUCT - Instituto de I&D em Estruturas e Construções - funded by national funds through the FCT/MCTES (PIDDAC); AARM4 - High Strength Steels in Metalmechanics 4.0 (POCI-01-0247-FEDER-068492) funded by national funds through the PT2020/COMPETE; and, individual project grant (2020.03856.CEECIND), awarded to José A.F.O. Correia, by national funds (PIDDAC) through the Fundação para a Ciência e Tecnologia (FCT/MCTES). This work is also a result of Agenda "NEXUS: Innovation Pact Digital and Green Transition – Transports, Logistics and Mobility", nr. C645112083-00000059, investment project nr. 53, financed by the Recovery and Resilience Plan (PRR) and by European Union - Next-Generation EU. Financial support from the National Natural Science Foundation of China (No. 12232004), China Scholarship Council (No. 202006070074) and Basic and Applied Basic Research Foundation of Guangdong Province (No. 2021B1515140030) are also acknowledged. Finally, Ding Liao gratefully acknowledges Dr. Jie-Wei Gao from the University of Electronic Science and Technology of China for his help on fracture surface analysis.

References

Aigner, R., Pusterhofer, S., Pomberger, S., Leitner, M., Stoschka, M., 2019. A probabilistic Kitagawa–Takahashi diagram for fatigue strength assessment of cast aluminium alloys. Mater. Sci. Eng., A 745, 326–334. https://doi.org/10.1016/j.msea.2018.12.108.

Alencar, G., De Jesus, A.M.P., Silva, J.G. S.d., Calçada, R.A.B., 2019. Fatigue cracking of welded railway bridges: a review. Eng. Fail. Anal. 104, 154–176. https://doi.org/10.1016/j.engfailanal.2019.05.037.

American Society for Testing and Materials, 2012. ASTM E606/E606M-12 Standard Test Method for Strain-Controlled Fatigue Testing, pp. 1–30. https://doi.org/10.1520/E0606_E0606M-19E01. America.

Basan, R., Franulović, M., Prebil, I., Kunc, R., 2017. Study on Ramberg–Osgood and Chaboche models for 42CrMo4 steel and some approximations. J. Constr. Steel Res. 136, 65–74. https://doi.org/10.1016/j.jcsr.2017.05.010.

Beretta, S., Foletti, S., Rusconi, E., Riva, A., Socie, D.F., 2016. A log-normal format for failure probability under LCF: concept, validation and definition of design curve. Int. J. Fatig. 82, 2–11. https://doi.org/10.1016/j.ijfatigue.2015.08.027.

British Standards Institution, B.S., 2019. 7910:2019: Guide to Methods for Assessing the Acceptability of Flaws in Metallic Structures, 8/16-8/18.

Chakherlou, T.N., Vogwell, J., 2003. The effect of cold expansion on improving the fatigue life of fastener holes. Eng. Fail. Anal. 10 (1), 13–24. https://doi.org/10.1016/S1350-6307(02)00028-6.

Chakherlou, T.N., Oskouei, R.H., Vogwell, J., 2008. Experimental and numerical investigation of the effect of clamping force on the fatigue behaviour of bolted plates. Eng. Fail. Anal. 15 (5), 563–574. https://doi.org/10.1016/j.engfailanal.2007.04.009.

Chakherlou, T.N., Mirzajanzadeh, M., Abazadeh, B., Saeedi, K., 2010. An investigation about interference fit effect on improving fatigue life of a holed single plate in joints. Eur. J. Mech. Solid. 29 (4), 675–682. https://doi.org/10.1016/j.euromechsol.2009.12.009.

Chen, H.X., Chen, Y.X., Yang, Z., 2014. Coupling damage and reliability model of low-cycle fatigue and high energy impact based on the local stress–strain approach. Chin. J. Aeronaut. 27 (4), 846–855. https://doi.org/10.1016/j.cja.2014.03.008.

Cheng, L., Yang, F., Winkes, J.S., Veljkovic, M., 2023a. The C1 wedge connection in towers for wind turbine structures, tensile behaviour of a segment test. Eng. Struct. 282, 115799 https://doi.org/10.1016/j.engstruct.2023.115799.

Cheng, L., Yang, F., Seidel, M., Veljkovic, M., 2023b. FE-assisted investigation for mechanical behaviour of connections in offshore wind turbine towers. Eng. Struct. 285, 116039 https://doi.org/10.1016/j.engstruct.2023.116039.

Conle, F.A., Chu, C.C., 1997. Fatigue analysis and the local stress–strain approach in complex vehicular structures. Int. J. Fatig. 19 (93), 317–323. https://doi.org/10.1016/s0142-1123(97)00045-5.

Correia, J.A.F.D.O., et al., 2017. Generalized probabilistic model allowing for various fatigue damage variables. Int. J. Fatig. 100, 187–194. https://doi.org/10.1016/j.ijfatigue.2017.03.031.

Creusen, K.E.Y., Misios, G., Winkes, J.S., Veljkovic, M., 2022. Introducing the C1 wedge connection. Steel Constr 15 (1), 13–25. https://doi.org/10.1002/stco.202100039.

Cuellar, S.D., Hill, M.R., Dewald, A.T., Rankin, J.E., 2012. Residual stress and fatigue life in laser shock peened open hole samples. Int. J. Fatig. 44, 8–13. https://doi.org/10.1016/j.ijfatigue.2012.06.011.

De Jesus, A.M.P., Da Silva, A.L.L., Correia, J.A.F.D.O., 2014. Fatigue of riveted and bolted joints made of puddle iron - a numerical approach. J. Constr. Steel Res. 102, 164–177. https://doi.org/10.1016/j.jcsr.2014.06.012.

Det Norske Veritas, 2014. DNV-RP-C203: Fatigue Design of Offshore Steel Structures, pp. 18–27.

Dias, J.P., et al., 2019. Parametric probabilistic approach for cumulative fatigue damage using double linear damage rule considering limited data. Int. J. Fatig. 127, 246–258. https://doi.org/10.1016/j.ijfatigue.2019.06.011.

Dong, C.L., Yu, H.C., Li, Y., 2015. Fatigue life modeling of a single crystal superalloy and its thin plate with a hole at elevated temperature. Mater. Des. 66 (A), 284–293. https://doi.org/10.1016/j.matdes.2014.10.071.

DuQuesnay, D.L., Topper, T.H., Yu, M.T., 1986. The effect of notch radius on the fatigue notch factor and the propagation of short cracks. In: Miller, K.J., Rios, E.R.D.L. (Eds.), The Behaviour of Short Fatigue Cracks. Mechanical Engineering Publications Limited, London, pp. 323–335.

Esmaeili, F., Chakherlou, T.N., Zehsaz, M., 2014. Prediction of fatigue life in aircraft double lap bolted joints using several multiaxial fatigue criteria. Mater. Des. 59, 430–438. https://doi.org/10.1016/j.matdes.2014.03.019.

European Committee for Standardization, 2005. Eurocode 3 - Design of Steel Structures - Part 1-9: Fatigue, pp. 14–17. Belgium.

Fan, Y.S., Yang, X.G., Tan, L., Sui, T.X., Shi, D.Q., Liu, H., 2022. Fatigue life evaluation for notched single-crystal Ni-based superalloys considering inhomogeneous rafting microstructure. Int. J. Fatig. 166, 107225 https://doi.org/10.1016/j.ijfatigue.2022.107255.

Feng, L.Y., Zhang, L.M., Liao, X.W., Zhang, W., 2021. Probabilistic fatigue life of welded plate joints under uncertainty in Arctic areas. J. Constr. Steel Res. 176, 106412 https://doi.org/10.1016/j.jcsr.2020.106412.

Fernández-Canteli, A.C., Blasón, S., Correia, J.A.F.D.O., De Jesus, A.M.P., 2014. A probabilistic interpretation of the miner number for fatigue life prediction. Frat. Ed. Integrità Strutt. 8 (30), 327–339. https://doi.org/10.3221/IGF-ESIS.30.40.

Fu, Y.C., De Ge, E., Su, H.H., Xu, J.H., Li, R.Z., 2015. Cold expansion technology of connection holes in aircraft structures: a review and prospect. Chin. J. Aeronaut. 28 (4), 961–973. https://doi.org/10.1016/j.cja.2015.05.006.

Gates, N.R., Fatemi, A., 2016. Fatigue crack growth behavior in the presence of notches and multiaxial nominal stress states. Eng. Fract. Mech. 165, 24–38. https://doi.org/10.1016/j.engfracmech.2016.08.017.

Gong, M., Zhao, J.H., Dong, B.H., Wang, X.F., Li, C.Z., 2002. Initiation and propagation of fatigue crack in edge region of hole in a sheet with central hole. Acta Aeronautica Astronautica Sinica 23 (3), 202–205.

Haldar, A., Mahadevan, S., 1999. Probability, Reliability, and Statistical Methods in Engineering Design. John Wiley & Sons, New York.

He, J.C., Zhu, S.P., Liao, D., Niu, X.P., Gao, J.W., Huang, H.Z., 2021. Combined TCD and HSV approach for probabilistic assessment of notch fatigue considering size effect. Eng. Fail. Anal. 120, 105093 https://doi.org/10.1016/j.engfailanal.2020.105093.

Kloos, K.H., 1976. Einfluss des Oberflächenzustandes und der Probengröße auf die Schwingfestigkeitseigenschaften.

Kuguel, R., 1961. A relation between theoretical stress concentration factor and fatigue notch factor deduced from the concept of highly stressed volume. Proceeding ASTM 61, 732–748.

Li, Y.Z., Zhu, S.P., Liao, D., Niu, X.P., 2020. Probabilistic modeling of fatigue crack growth and experimental verification. Eng. Fail. Anal. 118, 104862 https://doi.org/10.1016/j.engfailanal.2020.104862.

Li, G.C., Wang, Q., Zhong, G.Y., Xiao, F., 2022. Influence of assembly tolerance on fatigue reliability life of aircraft structures. Aero. Sci. Technol. 33 (3), 106–110. https://doi.org/10.19452/j.issn1007-5453.2022.03.014.

Liang, Y.P., Ren, X.D., Feng, D.C., 2022. Probabilistic safety assessment of nuclear containment vessel under internal pressure considering spatial variability of material properties. Int. J. Pres. Ves. Pip. 200, 104813 https://doi.org/10.1016/j.ijpvp.2022.104813.

Liao, D., Zhu, S.P., 2019. Energy field intensity approach for notch fatigue analysis. Int. J. Fatig. 127, 190–202. https://doi.org/10.1016/j.ijfatigue.2019.06.010.

Liao, M., Renaud, G., Bellinger, N., 2008. Probabilistic modeling of short-crack growth in airframe aluminum alloys. J. Aircraft 45 (4), 1105–1111. https://doi.org/10.2514/1.31649.

Liao, D., Zhu, S.P., Correia, J.A.F.D.O., De Jesus, A.M.P., Berto, F., 2020a. Recent advances on notch effects in metal fatigue: a review. Fatig. Fract. Eng. Mater. Struct. 43 (4), 637–659. https://doi.org/10.1111/ffe.13195.

Liao, D., Zhu, S.P., Keshtegar, B., Qian, G.A., Wang, Q.Y., 2020b. Probabilistic framework for fatigue life assessment of notched components under size effects. Int. J. Mech. Sci. 181, 105685 https://doi.org/10.1016/j.ijmecsci.2020.105685.

Liao, D., Zhu, S.P., Correia, J.A.F.D.O., De Jesus, A.M.P., Veljkovic, M., Berto, F., 2022. Fatigue reliability of wind turbines: historical perspectives, recent developments and future prospects. Renew. Energy 200, 724–742. https://doi.org/10.1016/j.renene.2022.09.093.

Liu, J., Yue, Z.F., Liu, Y.S., 2007. Surface finish of open holes on fatigue life. Theor. Appl. Fract. Mech. 47 (1), 35–45. https://doi.org/10.1016/j.tafmec.2006.10.008.

Liu, J., Lu, J., Wang, X., Sen Wang, X., Yue, Z.F., 2015. Corrosion fatigue performance of TC4 plates with holes in aviation kerosene. Aero. Sci. Technol. 47, 420–424. https://doi.org/10.1016/j.ast.2015.10.008.

Liu, X., Wang, R.Q., Hu, D.Y., Mao, J.X., 2020. A calibrated weakest-link model for probabilistic assessment of LCF life considering notch size effects. Int. J. Fatig. 137, 105631 https://doi.org/10.1016/j.ijfatigue.2020.105631.

Lukáš, P., Kunz, L., 1989. Effect of mean stress on cyclic stress–strain response and high cycle fatigue life. Int. J. Fatig. 11 (1), 55–58. https://doi.org/10.1016/0142-1123(89)90048-0.
Mäde, L., Schmitz, S., Gottschalk, H., Beck, T., 2018. Combined notch and size effect modeling in a local probabilistic approach for LCF. Comput. Mater. Sci. 142, 377–388. https://doi.org/10.1016/j.commatsci.2017.10.022.
Mohammadi, M., Rahmatfam, A., 2021. Low-cycle fatigue life prediction assessment of notched aluminum 2024-T3 under cyclic axial loading. Ships Offshore Struct. 1–11. https://doi.org/10.1080/17445302.2021.2007688.
Niu, X.P., Wang, R.Z., Liao, D., Zhu, S.P., Zhang, X.C., Keshtegar, B., 2021. Probabilistic modeling of uncertainties in fatigue reliability analysis of turbine bladed disks. Int. J. Fatig. 142, 105912 https://doi.org/10.1016/j.ijfatigue.2020.105912.
Pawliczek, R., Rozumek, D., 2020. Cyclic tests of smooth and notched specimens subjected to bending and torsion taking into account the effect of mean stress. Materials 13, 2141. https://doi.org/10.3390/ma13092141.
Pedrosa, B.A.S., et al., 2019. Fatigue resistance curves for single and double shear riveted joints from old Portuguese metallic bridges. Eng. Fail. Anal. 96, 255–273. https://doi.org/10.1016/j.engfailanal.2018.10.009.
Pedrosa, B., Correia, J.A.F.D.O., Rebelo, C.A.S., Veljkovic, M., 2020. Reliability of fatigue strength curves for riveted connections using normal and Weibull distribution functions. ASCE-ASME J. Risk Uncertain. Eng. Syst. Part A Civ. Eng. 6 (3), 04020034 https://doi.org/10.1061/ajrua6.0001081.
Rozumek, D., 2009. Influence of the slot inclination angle in FeP04 steel on fatigue crack growth under tension. Mater. Des. 30 (6), 1859–1865. https://doi.org/10.1016/j.matdes.2008.09.017.
Sanaei, N., Fatemi, A., 2021. Defects in additive manufactured metals and their effect on fatigue performance: a state-of-the-art review. Prog. Mater. Sci. 117, 100724 https://doi.org/10.1016/j.pmatsci.2020.100724.
Schijve, J., 1979. Four lectures on fatigue crack growth: I. Fatigue crack growth and fracture mechanics. Eng. Fract. Mech. 11 (1), 169–181. https://doi.org/10.1016/0013-7944(79)90039-0.
Schijve, J., 2009a. Fatigue and scatter. In: Fatigue of Structures and Materials, second ed. Springer, Berlin, pp. 373–394.
Schijve, J., 2009b. Fatigue of Structures and Materials, second ed. Springer Netherlands, Delft. https://doi.org/10.1007/978-1-4020-6808-9.
Singh, K., Sadeghi, F., Correns, M., Blass, T., 2019. A microstructure based approach to model effects of surface roughness on tensile fatigue. Int. J. Fatig. 129, 105229 https://doi.org/10.1016/j.ijfatigue.2019.105229.
Smith, K.N., Watson, P., Topper, T.H., 1970. A stress–strain function for the fatigue of metals. J. Mater. 5, 767–778.
Smith, I.F.C., 1986. Applying fatigue research to engineering design. In: Miller, K.J., Rios, E.R.D.L. (Eds.), The Behaviour of Short Fatigue Cracks. Mechanical Engineering Publications Limited, London, pp. 15–26.
Socie, D.F., 2003. Probabilistic Aspects of Fatigue. Urbana.
Soyama, H., Takeo, F., 2016. Comparison between cavitation peening and shot peening for extending the fatigue life of a duralumin plate with a hole. J. Mater. Process. Technol. 227, 80–87. https://doi.org/10.1016/j.jmatprotec.2015.08.012.
Stawiarski, A., 2018. The nondestructive evaluation of the GFRP composite plate with an elliptical hole under fatigue loading conditions. Mech. Syst. Signal Process. 112, 31–43. https://doi.org/10.1016/j.ymssp.2018.04.022.
Su, Y.L., Lu, S., Yang, M., Zhang, Q.B., 2018. "Probabilistic fatigue life model for medium and low cycle fatigue based on plastic strain energy (in Chinese). J. Aero. Power 33 (1), 62–68. https://doi.org/10.13224/j.cnki.jasp.2018.01.008.
Suhr, R.W., 1986. The effect of surface finish on high cycle fatigue of a low alloy steel. In: Miller, K.J., Rios, E.R.D.L. (Eds.), The Behaviour of Short Fatigue Cracks. Mechanical Engineering Publications Limited, London, pp. 69–86.
Suraratchai, M., Limido, J., Mabru, C., Chieragatti, R., 2008. Modelling the influence of machined surface roughness on the fatigue life of aluminium alloy. Int. J. Fatig. 32 (12), 2119–2126. https://doi.org/10.1016/j.ijfatigue.2008.06.003.
Susmel, L., Taylor, D., 2007. A novel formulation of the theory of critical distances to estimate lifetime of notched components in the medium-cycle fatigue regime. Fatig. Fract. Eng. Mater. Struct. 30 (7), 567–581. https://doi.org/10.1111/j.1460-2695.2007.01122.x.
Takakuwa, O., Takeo, F., Sato, M., Soyama, H., 2016. Using cavitation peening to enhance the fatigue strength of duralumin plate containing a hole with rounded edges. Surf. Coating. Technol. 307 (A), 200–205. https://doi.org/10.1016/j.surfcoat.2016.08.087.
Tan, Y., Wu, G., Yang, J.-M., Pan, T., 2004. Laser shock peening on fatigue crack growth behaviour of aluminium alloy. Fatig. Fract. Eng. Mater. Struct. 27 (8), 649–656. https://doi.org/10.1111/j.1460-2695.2004.00763.x.
Taras, A., Greine, R., 2010. Development and application of a fatigue class catalogue for riveted bridge components. Struct. Eng. Int. 20 (1), 91–103. https://doi.org/10.2749/101686610791555810.
Valtinat, G., Hadrych, I., 2000. Strengthening of riveted and bolted steel constructions under fatigue loading by preloaded fasteners-experimental and theoretical investigations. In: Proceedings of the International Conference on Connections in Steel Structures IV, AISC and ECCS, pp. 464–473. Roanoke.
Visvanatha, S.K., Straznicky, P.V., Hewitt, R.L., 2000. Influence of strain estimation methods on life predictions using the local strain approach. Int. J. Fatig. 22 (8), 675–681. https://doi.org/10.1016/S0142-1123(00)00042-6.
Wang, R.Q., Li, D., Hu, D.Y., Meng, F.C., Liu, H., Ma, Q.H., 2017a. A combined critical distance and highly-stressed-volume model to evaluate the statistical size effect of the stress concentrator on low cycle fatigue of TA19 plate. Int. J. Fatig. 95, 8–17. https://doi.org/10.1016/j.ijfatigue.2016.10.003.
Wang, Z.Y., Wang, Q.Y., Li, L.H., Zhang, N., 2017b. Fatigue behaviour of CFRP strengthened open-hole steel plates. Thin-Walled Struct. 115, 176–187. https://doi.org/10.1016/j.tws.2017.02.015.
Wang, R.Q., Liu, H., Hu, D.Y., Li, D., Mao, J.X., 2018. Evaluation of notch size effect on LCF life of TA19 specimens based on the stress gradient modified critical distance method. Fatig. Fract. Eng. Mater. Struct. 41 (8), 1794–1809. https://doi.org/10.1111/ffe.12821.
You, B.R., Lee, S.B., 1996. A critical review on multiaxial fatigue assessments of metals. Int. J. Fatig. 18 (4), 235–244. https://doi.org/10.1016/0142-1123(96)00002-3.
Zhi, Y.L., et al., 2022. Improvement of traction-traction fatigue properties of A100 steel plate-hole-structure by double shot peening. Int. J. Fatig. 162, 106925 https://doi.org/10.1016/j.ijfatigue.2022.106925.
Zhu, S.P., Foletti, S., Beretta, S., 2017. Probabilistic framework for multiaxial LCF assessment under material variability. Int. J. Fatig. 103, 371–385. https://doi.org/10.1016/j.ijfatigue.2017.06.019.